European Pressurized Reactor (EPR)

SH2702 Nuclear Reactor Technology

Emma Dubald

Genevieve Erjavec

Group 43

Contents

1. Introduction

The European Pressurized Reactor (EPR) is a Generation III pressurized water reactor (PWR). The EPR was developed in a collaboration between Électricité de France (EDF) and Framatome in France, and Siemens in Germany. The design of the EPR is based on decades of research and operating experience from former light water reactors, specifically building upon the designs of the N4 and KOVOI French and German reactors. The first commercial EPR began operation in 2018 in Taishan, China. There are currently two units operating at Taishan and more under construction in Finland, France, and the UK. EPRs have been associated with significant delays and cost overruns; the EPRs in Olkilutot, Finland, and Flamanville, France, had 14 and 11-year operational delays, respectively. As such, EDF started working on the design of the EPR2 in 2015 to address these challenges [1]. The design philosophy of the EPR is based on three goals: improve safety levels (considering both probabilistic and deterministic), mitigate severe accidents by limiting their consequences to the plant, and reduce power generation costs [2].

2. General Design Specification

The EPR is a light water moderated and cooled pressurized water reactor (PWR). The reactor coolant system (RCS) design features a four-loop system, and the main components are: a reactor vessel housing the reactor core, a pressurizer, one reactor coolant pump per loop, and one steam generator per loop, as presented in the reactor configuration presented in Figure 1. The EPR has an electrical output of 1600 MW with a 36-37% overall efficiency. It is expected to have a 60-year service life and an average availability factor up to 92% [3] [4]. The following section highlights the main components of the EPR.

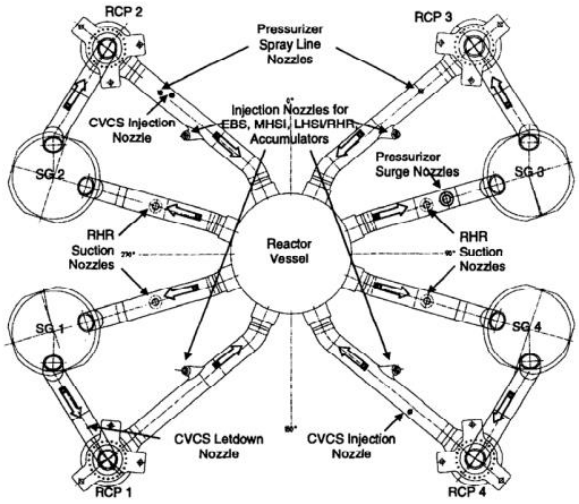

Figure 1- Schematic of EPR RCS Configuration

2.1. Core

The fuel assembly features a 17 x 17 square lattice, where the fuel rods are held in place by ten high thermal performance spacer grids and two end spacer grids. The spacer grids have integrated mixing vanes for optimal heat transfer between the cladding and coolant. The fuel rods contain a stack of sintered pellets composed of either uranium oxide with enrichment up to 5 wt% or uranium and plutonium mixed oxide (MOX) fuel. The active fuel length is 4.2 m,

and a 2 – 8 wt% Gd_2O_3 burnable poison can be integrated with the fuel to absorb neutrons when there is excess reactivity in the fresh fuel. A plenum is present inside the fuel rod to minimize pressure build-up due to the release of fission product gases. Twenty-four positions in the assembly have guide thimbles, which are used as locations for the Rod Cluster Control Assemblies (RCCAs). Fuel management flexibility is achieved by the 180-degree rotational symmetry of the fuel assembly. The top and bottom nozzles provide structural support for the assemblies. Further, the top nozzle prevents hydraulic lift-off of the fuel assembly by supporting the hold-down springs while the bottom nozzle distributes the coolant flow and filters out debris in the coolant [3] [4]. The reactor core contains 241 fuel assemblies. A schematic of the EPR fuel assembly is presented in Figure 2.

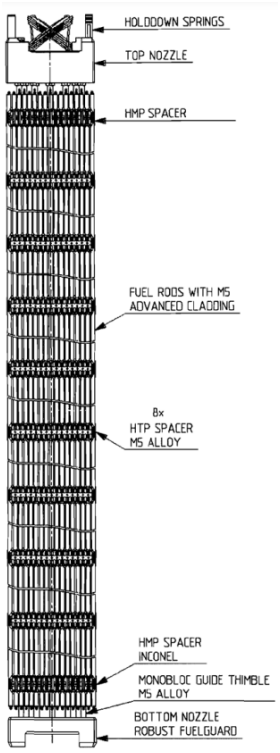

Figure 2- Schematic of EPR Fuel Assembly

The fuel rod cladding, guide thimbles and spacer grids are composed of Framatome's M5 zirconium-based alloy, which is currently the most advanced PWR material. It has high corrosion resistance and dimensional stability, low hydrogen up-take, and desirable behaviour during power ramp-ups, loss of coolant accident (LOCA) and reactivity insertion accident situations [3] [4].

The reactor contains eighty-nine RCCAs, each containing twenty-four absorber rods in a spider assembly. The rods are composed of stainless-steel tubing containing neutron absorbing materials; the material in the lower part of the rod is an Ag-In-Cd alloy and the upper part is boron carbide. The rapid shutdown system utilizes all of the RCCAs [3].

The key feature of the EPR reactor core is its flexibility for various fuel management strategies, extended fuel cycle length (leading to reduced costs), and high thermal efficiency. The EPR reactor design has increased margins which provide flexibility of in-core fuel management strategies and cycle length durations, and reductions in fuel cycle costs. The most commonly used fuel scheme is in-in-out, but other schemes like out-in-in and in-out-in can also

be used. The average discharge burn-up is up to 60 GWd/MTU (compared to a typical PWR burnup of about 45 GWd/MTU) [5]. The EPR core design can achieve up to 50% plutonium recycling of the MOX in-core fuel assemblies. Further, the heavy (8 – 30 cm) stainless steel reflector located between the core and core containment maximize the neutron economy, thus increasing the fuel cycle length or reducing the fuel enrichment requirement [3].

2.2. Reactor Pressure Vessel

The reactor pressure vessel (RPV) houses the reactor core, control rods, reflector, and internal components to direct flow. It is a cylindrical vessel composed of low-alloy steel. To provide corrosion resistance, the inner surface is coated with stainless steel cladding. It has four inlet and four outlet nozzles located below the RPV flange and above the top of the core. Coolant enters the RPV through the inlet nozzles, where it then flows downwards through the downcomer until it reaches the bottom of the vessel. The coolant is then directed upwards where it flows through the core to the outlet nozzles, where it is sent to the steam generator (SG) [3].

The RPV is divided into lower and upper sections. The lower section internals consist of the core barrel, the lower core support structure, the reflector and the flow distribution device. The core barrel houses the reactor core and is made from several cylindrical pieces welded together. Its upper sections contains four outlet nozzles to direct the coolant flow from the core to the RPV outlet nozzles. It houses irradiation capsule baskets for brittle fracture monitoring following the irradiation of materials inside the reactor. The lower support plate provides structural support for the RPV internals and is welded to the bottom of the core barrel, supporting the fuel assemblies, reflector and flow distribution device. The flow distribution device is placed below the lower support plate and contains holes to evenly distribute coolant to the core inlet. The heavy reflector is a unique feature of the EPR RPV. Located inside the core barrel, the heavy reflector improves neutron economy by reducing fast neutron leakage and evenly distributing neutron flux. It is made of stainless steel rings stacked on top of one another to avoid welded connections. Coolant channels in the heavy reflector prevent structural stress of the material due to heat production from absorption of gamma rays in the reflector. The closure head of the vessel has penetrations welded for adapters for control rod drive mechanisms (CRDM), measurement probes, instrumentation, and detectors [3].

The upper section internals consist of the upper support plate, the upper core plate and other support columns. The upper support plate is a thick plate separating the core barrel upper plenum from the upper head dome of the vessel itself and compressing the fuel assemblies. The upper core plate is a perforated austenitic stainless steel plate and aligns the fuel assemblies and RCCA guides. The upper support plate and upper core plate are connected by the support columns for the RCCA guides and normal support columns. A schematic of the RPV is presented in Figure 3 [3].

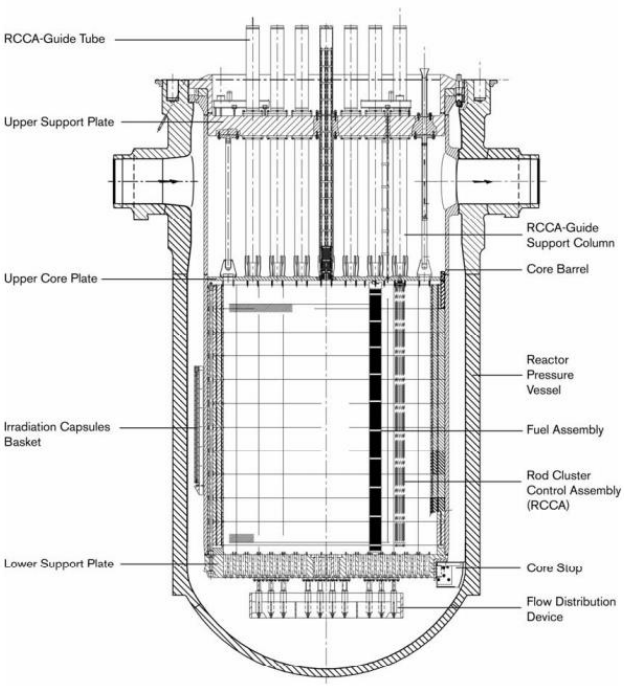

Figure 3 - Schematic of EPR RPV

2.3. Pressurizer

The pressurizer is a vertical cylinder with hemispherical ends composed of ferritic steal with austenitic stainless steel cladding on the inner surfaces. The pressurizer maintains the pressure and volume in the RCS of PWRs to prevent boiling. The pressurizer volume contains saturated water and steam and the pressure is controlled by varying the temperature of coolant via two systems: the spray system and the electric heater system. To increase the pressure in the RCS, the electric heater system is turned on to increase the temperature and evaporate some of the water, thus increasing the pressure in the pressurizer and the RCS. The RCS pressure is decreased by activating the spray system to condense some of the steam and decrease the pressure in the pressurizer. In addition to maintaining the system pressure, the pressurizer monitors water level in the RCS and is an over-pressure relief system [3].

In the EPR pressurizer, the spray system consists of two main spray nozzles on either side of the pressurizer connected to the cold leg, and one auxiliary spray nozzle connected to the containment vessel cooling system, all of which are located at the top of the pressurizer. The electric heater system is made up vertical heated rods which are in the bottom head. On the upper head, the relief system consists of three safety valves, which are actuated by the pressure sensors in the upper shell and sensing nozzles in the steam volume. The upper head also has one nozzle for the pressurizer depressurization system line in case of severe accident, a vent nozzle, and a manway to provide access for maintenance. The surge line connects the RCS to the pressurizer nozzle vertically by one hot leg. A schematic of the EPR pressurizer is presented in Figure 4 [3].

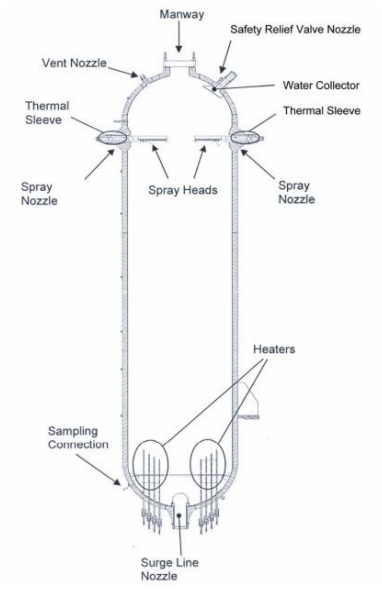

Figure 4 - Schematic of EPR Pressurizer

2.4. Steam Generators

The steam generators (SGs) are vertical shell U-tube heat exchangers operating on the principle of natural circulation. The primary coolant enters and exits through nozzles at the bottom of the SG. The heat from the coolant is transferred through the tube walls to the secondary loop on the shell side of the heat exchanger at a lower pressure, generating steam. A schematic of the EPR SG is presented in Figure 5 [3].

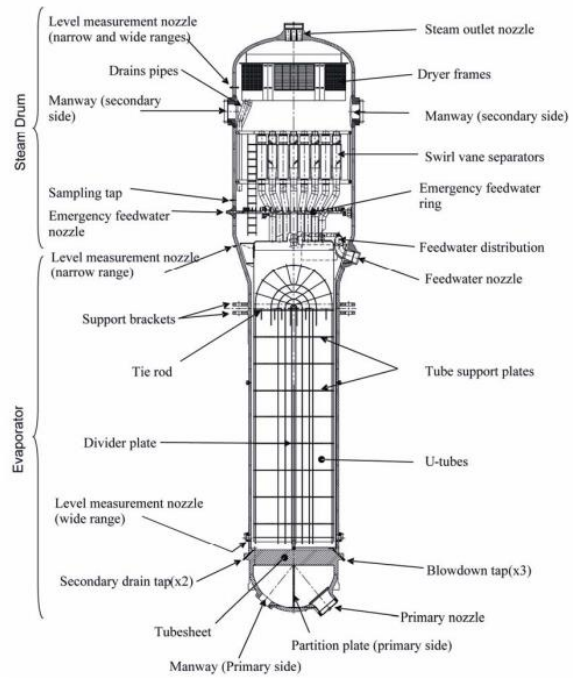

Figure 5 - Schematic of EPR Steam Generator

A unique feature of the EPR SG is the axial economizer. The operating principle of the axial economizer is presented in Figure 6 [4].

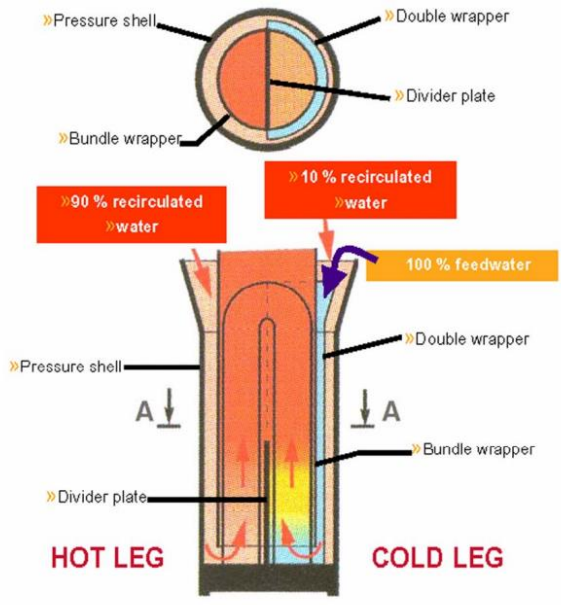

Figure 6 - Operating Principle of Axial Economizer in EPR

The double wrapper divides the downcomer of secondary side feedwater into two parts, the hot and cold sides of the tube bundle, and the partition plate divides the lower part of the tube bundle into the hot and cold sides. All the secondary side feedwater and 10% of recirculated water from the moisture separators is distributed to the cold side, and the remaining 90% of recirculated water enters the hot side due to the double wrapper. The secondary side feedwater distribution system covers only about one half of the cold side. It flows down through the double wrapper and once it reaches the bottom, it switches direction and flows upwards along the cold side tube bundle between the wrapper and partition plate, where it is heated to create steam. Since the feedwater is not mixed with all the recirculation water as it would be without the axial economizer, the secondary side feedwater temperature is lower, resulting in an increased average temperature difference between the primary and secondary side. Thus, the heat transfer is improved which increases the outlet steam pressure by approximately 3 bar when compared to other SGs of the same heat exchange area. This is a large contributor to the improved efficiency of this reactor when in comparison to other PWRs. The SG tubes are made from Inconel 690, a highly corrosion-resistant material used worldwide. Low alloy ferritic steel is used for the secondary shell [3] [6].

2.5. Reactor Coolant Pumps

The reactor coolant pumps (RCPs) are vertical shaft, single stage, suction diffuser type pumps driven by air-cooled three-phase induction motors. There is one reactor coolant pump on each loop, for a total of four pumps, which transfer the primary coolant from the outlet of the steam generator to the inlet of the reactor core. The primary parts of the RCPs are the hydraulic section, the motor, and the shaft seal system. The shaft seal system contains three dynamic seals to prevent coolant leakage as a typical PWR does, however, the EPR also has a standstill seal. It ensures sealing in the cases of the loss of the water supply used to cool the shaft sealing system, cascaded failure of the other stages of the shaft sealing system, or station blackout (SBO). The standstill seal is actuated following the seal closure of the leak-off lines

and once the pump is at rest. Nitrogen pressure moves a ring seal, closing against a landing on the rotor and creating a sealing surface with metal-to-metal contact [3] [4].

2.6. Plant Layout

The plant layout and containment structure of the EPR makes is extremely resistant to external hazards, such as earthquakes are plane crashes. The reactor building in the centre houses the RCS and in-containment refueling water storage tank (IRWST) and has a double layer containment: the inner containment building (pre-stressed concrete shell with a steel liner) and a reinforced concrete shield building. A reinforced concrete compartment next to the reactor building protects the main steam and feedwater valves. Further, there are concrete walls separating the pressurizer, each loop, and their hot and cold sides. The four trains of the safety systems are in four separate safeguard buildings surrounding the reactor building. Each safeguard building contains a separate emergency diesel generator (EDG) so the safety systems can operate if AC power is lost, and two of the safeguard buildings are protected against extreme external hazards. There are also two separate buildings containing EDGs in case of SBO [4] [3]. The EPR plant layout is presented in Figure 7 [4].

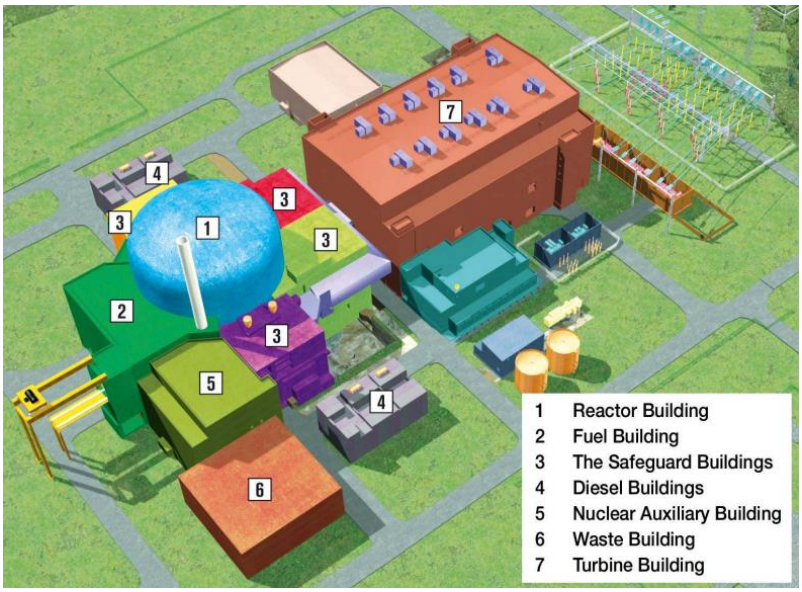

Figure 7 - Plant Layout of EPR

2.7. Balance of Plant

2.7.1. Main Steam System

The main steam system (MSS) begins at the outlet of the SGs and pipes the steam to the high-pressure turbine which, together with the low-pressure turbines, drive the electric generator. Following expansion in the high-pressure turbine, the steam is routed to two moisture separator/reheater units, where it is dried and reheated. The resulting steam is sent to three double-flow low-pressure turbines, driving the electric generator. The steam exiting each low-pressure turbine is sent to a condenser, operating at vacuum conditions to maximize energy removal by the low-pressure turbines. Water circulating through the condenser tubes condenses the steam into water which is collected at the hotwell area of the condenser. Condensate pumps raise the pressure of the water which is then passed through a cleanup system to remove impurities, so they do not accumulate in the SGs. A series of four low-pressure feedwater heaters raise the temperature of the condensate using extraction steam from the low-pressure

turbines. The main feedwater pumps raise the pressure to the SG operating pressure and the feedwater then passes through two high-pressure feedwater heaters, heated with extraction steam from the high-pressure turbine. The feedwater then re-enters the bottom of the SG through the main feedwater inlet nozzles. The main feedwater line is equipped with isolation and control valves [3].

The main steam line from the SGs to the high-pressure turbine is equipped with a main steam isolation relief valve (MSIRV) right outside the containment, and overpressure protection is accomplished by a main steam relief train (MSRT) and two main steam safety valves (MSSVs). The MSIRVs are closed during normal operation and are fast opening valves in the case of overpressure. The MSSVs are open during normal operation and stop flow through a MSIRV which is stuck open. If there is an imbalance between turbine load and power or a reactor trip, turbine bypass valves actuate to allow excess steam to be dumped directly to the main condenser [3].

2.7.2. Main Feedwater System

The main feedwater system supplies feedwater to the SGs during normal operation. It consists of the feedwater tank, feedwater pumps, high pressure feedwater heaters, and feedwater isolation valves. Feedwater is pumped from the feedwater storage tank to two high pressure feedwater heaters which are heated by the turbine extraction steam. This condensed steam is routed back to the feedwater tank. The heated feedwater is sent to the SG inlet nozzles. Closure of the main feedwater isolation valve and full-load and low-load isolation valves during accident scenarios provides reactivity control by mitigating an overcooling transient due to overfeeding the SGs. The isolation valves have emergency backup power so they can function during SBO scenarios [3].

3. Operational Principles

The way in which a reactor is started, operated and controlled under normal conditions, and shutdown is integral to its design and overall safety. In this section, these methods are described. Further, the auxiliary systems of the EPR are introduced.

3.1. Reactor Operation During Start-up, Normal Conditions, and Shutdown

3.2.1. Start Up and Normal Operation

Following fuel loading, the RPV is closed by a multi-stud tensioning machine and electrical connection of the control rods and core instrumentation are installed. Start up the reactor is described by the following steps [7]:

1. Filling the primary coolant system:
    a. A vacuum is created in the primary system to minimize the air content in the primary coolant. This is to prevent fuel damage from fuel rod contact with air.
    b. 75% of the system is filled with reactor boron and water makeup. The filling of the primary coolant is stopped when the pressurizer level reaches about 90% of the range.
2. Heating the primary coolant:
    a. The flow rate in the safety facilities is increased to its standard value.
    b. The pressure into the primary coolant system is increased to 25 bar so the primary reactor coolant pump can be started.

c. The primary coolant temperature is then increased to 90°C. At this temperature, hydrazine is added to reduce the concentration of oxygen in the primary circuit to prevent from explosion. Once the primary coolant fulfilled all these requirements, the bubble is formed in the pressurizer and its pressure control is switched into two-phase mode.
d. The primary coolant is heated to 120°C. Above this temperature, the four steam generators are available and the secondary system is made available.

Steps 1 and 2 place the reactor into hot shutdown mode. To transition from hot shutdown mode to power operation, Steps 3 and 4 are followed:

3. Checking test are performed. This includes tests to measure the rod drop time or tests at zero power of the primary coolant diluted with demineralised water.
4. Power is increased by controlling the flux level. When the power is at 25% of nominal power the rod control system is put in automatic mode, “average temperature control mode”.

The power distribution is assessed with the aeroball system. It consists of stacks of vanadium that are inserted from the top of the reactor vessel into the reactor core inside the guide thimbles of the fuel assemblies. The time periods necessary for a flux measurement are 3 minutes for activation, followed by 5 minutes for reactivity measurements. This system, therefore, allows flux-mapping measurements in time intervals of 10 to 15 minutes. The normal operational condition for a reactor is defined as the production of constant power within the safety limits established for the plant and respecting the scheduled maintenance. [3]

3.2.2. Shutdown

A benefit of the EPR is that it was built to allow efficient refuelling to increase the overall capacity of the plant. Further, maintenance and inspection of equipment is simplified. During operation, the reactor building is designed to be accessible, under normal safety and radiation protection conditions. Thus, the preparation of maintenance missions does not require the shutdown of the reactor. Maintenance and refuelling operations can be started up to 7 days before the shutdown of the reactor, which allows for critical time saving. The last operations that must be performed for fuel loading or maintenance can still be performed up to three days after the restart of the reactor. Thus, the duration of the shutdown and restart phases are reduced; they are assumed to be 70 and 90 hours, respectively. The operations of loading/unloading of fuel are estimated to last about 80 hours. With EPR technologies, the duration of a regular shutdown for preventive maintenance and fuel replacement is estimated at 16 days, as compared to 30 days with other reactor types [4]. Fuel reloading in EPRs is simplified by, for example, the use of larger fuel handling machines. This reduces manual handling and makes the refuelling process faster and more efficient. The fuel assembly storage and handling areas are also very close to the reactor. Finally, some PWR facilities may also use software to manage the refuelling process, including scheduling, inventory management and documentation. This streamlines the process, reducing the risk of errors and increasing efficiency.

A shutdown for refuelling only (without maintenance operations) can even be reduced to a maximum of 2 days. The ten-yearly shutdowns scheduled for in-service inspection of the main

equipment, turbine overhaul and pressure testing of the containment are planned to last 38 days. The shutdown mode of the plant (hot shutdown or residual heat removal system shutdown) will depend on the nature of the intervention and its duration. During an extended hot shutdown, the boron concentration in the primary circuit is adjusted according to the fuel burnup and the duration of the shutdown. Hot shutdowns are not possible for fuel replacement, and in this case a cold shutdown is performed. [4]

The reactor shutdown is initiated by reducing the turbine load. The power level for grid disconnection and turbine shutdown varies depending on the type of pumps used. In order to reduce the flow in the reactor, the control rod system also changes its mode. During normal operation, the system is in the "average temperature control" mode and during shutdown, the system switches to the "flux level control" mode to reduce the flux to 25% of the nominal power. 25% of the nominal power is the power limit at which the turbine can be disconnected. After the turbines are shut down, the control rods are manually inserted to completely shut down the reactor.

After shutdown, the temperature of the primary coolant is controlled by the turbine bypass system. The steam generators remain on, and their water level is controlled by the start-up and shutdown systems and the feedwater flow control system. The primary system is borated to maintain the required shutdown margin. Hot shutdown tests and inspections are performed. For shutdowns that require the reactor to be cold, that means temperature smaller than 100°C and pressure around the atmospheric one, the primary circuit is gradually cooled via the primary pumps which circulate the fluid in the steam generators. The maximum cooling rate of the system is 50°C per hour. In parallel, the pressurizer is also used to reduce the pressure within the reactor to around 25 bars. After stopping the last primary pump, the primary fluid, in the solid water phase, is depressurized to atmospheric pressure. [3]

3.3. Reactivity Control

Reactivity control is managed in two different ways: control rods and modification of the reactor coolant boron content. The EPR control mode is called the mode T and it is completely self-acting and it can influence 3 parameters through control loops: mean temperature, axial offset and power. The power variations can be performed at 5%/mn in the range 100%-60% of nominal power and at 2.5%/mn in the range 60%-25% nominal power [3], [8].

The variation of boron concentration in the primary coolant is used to compensate the slow reactivity changes caused by xenon and burnup. This is done by gradually diluting the primary coolant to a boron concentration ranging from 5 to 10 ppm at the end of the fuel cycle. The decrease in reactivity due to fuel depletion may also be compensated by reducing the primary coolant temperature. [3]

When there are fast reactivity changes or when the power level should be changed, the control rods are used. Control rod operation for reactivity control works automatically and rods can be in different modes. During normal operation, the control rods are in the mode “temperature and power distribution control” and can be inserted or extracted by core regulation.

The EPR core contains 89 control rods that are divided into shutdown groups. There are 5 groups of control rods that are then split into 2 major banks: Pbank and Hbank. The way they are distributed depends on the power configuration of the reactor. The Pbank section is used for temperature control and mainly to compensate important reactivity changes. Pbank rods

will be inserted when reactor temperature is too high and removed when temperature is too low. The Hbank section is used for axial offset control. Figure 8 presents a typical configuration of the control rod banks during a change of reactor power [8].

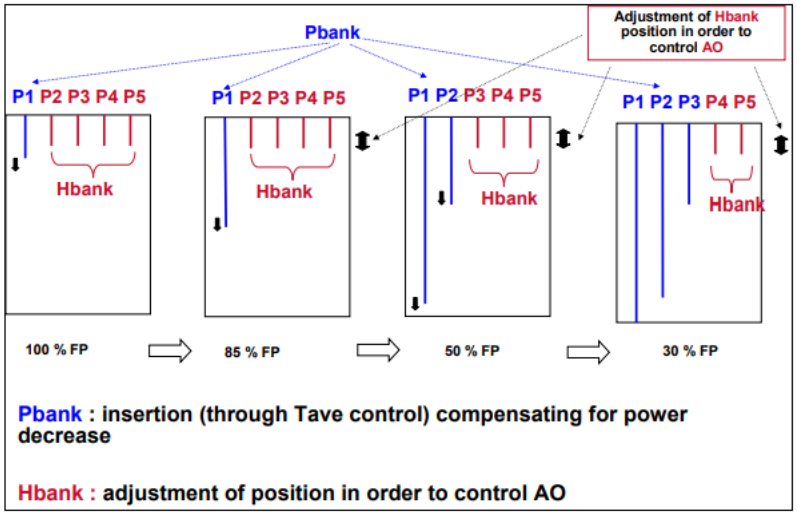

Figure 8 - Example configuration of control rod groups in EPR [8]

3.4. Auxillary Systems

The auxiliary systems include the nuclear operational systems, the maintenance area and laboratories. They are critical systems which support the main reactor and ensure safety, reliability, and efficiency. The nuclear auxiliary building contains the auxiliary system required for normal reactor operation which are described in the sections below [9].

3.4.1. Chemical and Volume Control System

This system regulates and adjusts the boron content in the primary system to regulate the power variation. During an accident, this system prevents boron-related accidents such as heterogeneous dilution accidents or the consequence of a homogeneous dilution. It also must ensure auxiliary spray in the pressurizer [10].

3.4.2. Gaseous Waste Processing System

This system is used to treat the gases that escape from reactor coolant and to collect radioactive waste gases. Waste gases are a product of fission product gases and radiolytic decomposition gases that are generated during fission. This system is maintained at negative pressure levels to prevent the escape of gases, in addition to limiting the coolant oxygen concentration to less than 0.1% to minimize neutron absorption in oxygen. [9]

3.4.3. Reactor coolant effluent processing system

This system treats the liquid radioactive discharges due to the reactor operation. The waste are produce in the core of the reactor and then transported through the reactor by the coolant. The effluent management process consists of collecting the waste, processing them and then do the storage and the disposal of the waste. The liquid effluents are mostly due to activated corrosion product that are presented in the structure of the primary circuit; the liquid effluent is treated by evaporation, degassing or filtration. [9]

3.4.4. Boron recycling system

This system recovers the excess boric acid from plant operation. The borated water is collected in a tank which is pumped by a boric acid evaporator feed pump through a filter. The liquid

then goes to the evaporation section where the evaporator separates the fluid into water vapor and a concentrated boric acid solution. The water vapor rises through the absorption tower, where any boric acid or gas carryover is absorbed by the recirculated condensate (reflux) flow and returned to the evaporator section. The remaining water vapor is condensed in the evaporator condenser and pumped through an evaporator condensate demineralizer [3].

4. Safety Features

The design of the EPR is based on that of previously successful PWRs, however there has been significant innovations in safety, mainly regarding core meltdown prevention and the mitigation of its associated consequences. The concept of defence-in-depth has been used by identifying potential accidents and implementing multiple protective barriers to prevent them from occurring. In the case of the EPR, the first level of defence-in-depth is achieved by a high-quality reactor design and lessons learned from operational experience of previous reactors. The second level involves surveillance and detection of variations from normal operating conditions to foresee potential failures as soon as possible. The third level of defence-in-depth is the control of design basis accidents and the prevention of their progression, and the fourth level is the control of severe accident conditions and the prevention of core meltdown. Defense-in-depth is achieved through redundancy and diversification of the implemented safety systems and physical barriers including the fuel pellets, cladding, primary circuit boundary, and containment. Regulations state that cumulative core damage frequency must be less than 10^{-5} per reactor-year and cumulative large release frequency of radioactivity to the environment from a core damage event < 10^{-6} per reactor-year and the EPR meets these requirements [4].

4.1. Safety Injection / Residual Heat Removal

The safety injection system/residual heat removal system (SIS/RHRS) is multi-functional; during normal operation, the RHRS provides shutdown cooling. The safety function of SIS is the removal of decay heat and emergency coolant injection following a LOCA. Further, a steam generator tube break or loss of secondary-side heat removal would actuate the system. The system has four independent trains (corresponding with the four-loop RCS), each with a nitrogen gas pressurized accumulator, a medium head safety injection (MHSI) pump, low head safety injection (LHSI) pump, and the IRWST. The redundancy of the four-train safety systems allows one train to be out of service for maintenance purposes, one to fail operation, and there are still two remaining to perform the required safety function [3].

When the RCS pressure falls below the accumulator pressure, the contents of the accumulator is injected at high speed into the RCS. The MHSI and LHSI pumps take suction from the IRWST and inject into the cold leg of the RCS. The LHSI can be switched over to the hot leg in the long term to prevent boron crystallization in the upper core. Downstream of each LHSI pump is a heat exchanger, cooled by the component cooling water system [3].

The IRWST is an open tank located at the bottom of the containment containing a large volume of borated water and collects water from inside the containment. Its function during normal operation is to flood the refuelling cavity during refuelling. Its safety function is to provide water for the SIS in the event of a LOCA, and containment and core melt cooling during severe accident conditions. The four SIS trains each have a sump suction connection to the IRWST. The floor beneath the RCS has openings to drain water released during the LOCA to the IRWST. The openings are equipped with retaining baskets to prevents debris from entering. The IRWST components are all passive besides the sump suction isolation valves

which are powered by safety-related buses. The other components of the SIS/RHRS trains are active but are powered by separate emergency buses which have EDGs for backup. Two trains also have SBO diesels for backup [3]. A schematic of the SIS/RHRS is presented in Figure 9 [4]

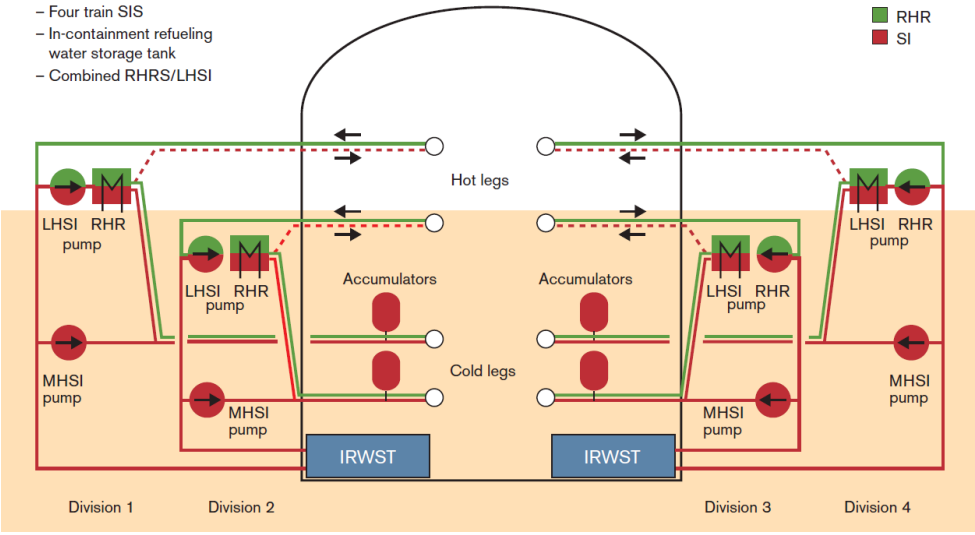

Figure 9 - Schematic of SIS/RHRS

4.2. Emergency Feedwater System

The purpose of the emergency feedwater system (EFWS) is to provide a sufficient supply of water to the SGs following a LOCA or SG tube break. In addition, it ensures heat transfer from the RCS to the atmosphere in a case of a different type of accident. Similar to the other systems mentioned, the EFWS has four independent trains consisting of an emergency pump taking suction from an EFWS storage tank, with lines equipped with control and isolation valves. The capacity of the system is such that it can remove the decay heat following a reactor trip from full power. Each train is powered by a separate emergency bus, each of which are backed up by an EDG. Two trains can be powered by the SBO DGs. A schematic of the EFWS is presented in Figure 10 [3].

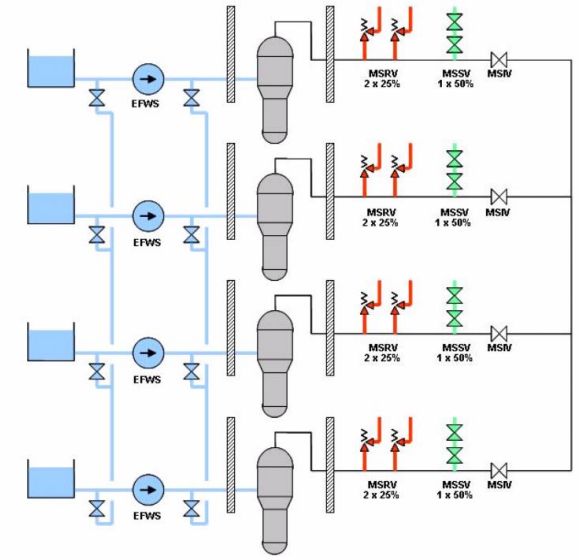

Figure 10 - Schematic of EFWS in EPR

.

4.3. Emergency Diesel Generators

In case of external electrical loss of power the EDGs should be used in order to restore the power supply to the diesel generators providing power to the safety systems. For the EPR the diesel generators allowed to function at full load for 72 hours [11].

4.4. Building and containment

The EPR features a double wall containment as illustrated in Figure 11 [11].

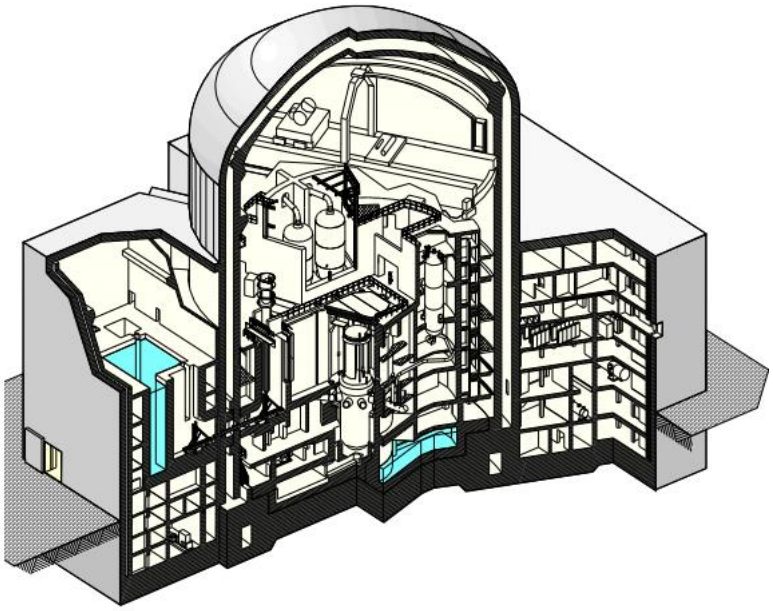

Figure 11 - Schematic of EPR Containment

The aim of the containment is to protect the reactor from possible damage caused by external sources (plane crash, earthquakes, etc.) and to protect humans and the environment from

radiation. The annulus between the two containments is filled with air under vacuum so as to suck out any leaks that may occur. There is a ventilation system that collects and filters any leaks coming from the internal wall before they are released into the atmosphere (absolute filters and iodine traps). It is calibrated to have a maximal depressurization of approximately 15mBar. The rate of leakage from the internal enclosure should not exceed 0.3% per day of the mass of gas mass contained in the inner vessel in case of loss of primary coolant and core meltdown accidents. The rate of leakage from the external wall should not exceed 1.5% per day of the of the total mass of gas contained in the annular [11].

Both walls from the double wall containment are made of concrete and have thicknesses of 130 cm and 180 cm, respectively. The inner wall has a steel liner (roughly 0.74 cm thick) on its part that is the closest to the reactor vessel, preventing corrosion. The outer wall is made of pre-stressed concrete to protect the reactor from external threats, such as earthquakes and plane crashes [11].

4.5. Containment Heat Removal System

The containment heat removal system (CHRS) is used to regulate the pressure and temperature inside the reactor containment building and cool the IRWST and spreading compartment in the case of severe accident. The system is comprised of two separate, identical trains, each consisting of a suction line from the IRWST, and a pump and heat exchanger located in safeguard buildings. The system consists of three different flow paths. The first is the dome spraying system which contains spray nozzles in the dome at the top of the reactor used to lower the containment temperature and pressure and condense airborne fission products. This system is used short term following a severe accident, however, the operation mode can be switched to use this system longer term if necessary. The second flow path is used for decay heat removal from the spreading compartment. Water from the IRWST is used to flood the spreading compartment and the steam generated from this is condensed back into the IRWST from the containment atmosphere. A flow limiter is used to prevent backflow to the IRWST. Lastly, sump screen flushing device removes debris accumulation from the CHRS pump suction nozzle sump screens. A schematic of the CHRS is presented in Figure 12 [3].

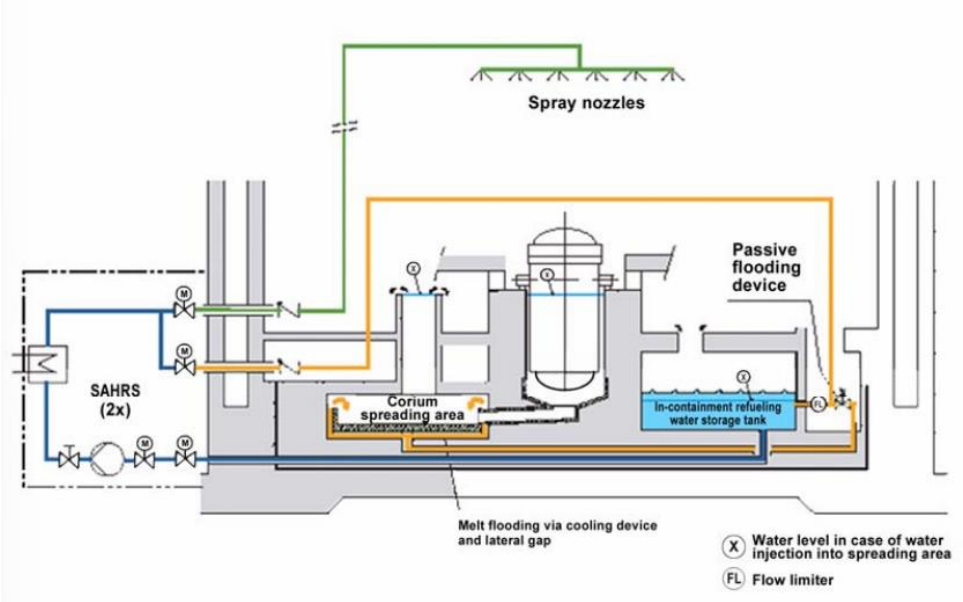

Figure 12 - Schematic of the CHRS in EPR

4.6. Combustible Gas Removal System

The combustible gas control system (CGCS) is a fully passive system whose purpose is to limit the hydrogen concentration during LOCAs and severe accidents to mitigate the risk of hydrogen explosion. It maintains the containment integrity and reduces the likelihood of radioactive releases to the environment by preventing excessive loads on the containment structure. The zinc-water reaction of zirconium cladding at high temperatures generates hydrogen. The system is normally in standby mode and begins operating when exposed to a hydrogen environment. The CGCS consists of passive autocatalytic recombiners (PARs), rupture foils and hydrogen mixing dampers. The PARs are rectangular-shaped devices with catalyst-coated plates (typically platinum) located at the bottom which react with hydrogen. The oxygen and hydrogen reaction creates heat and generates steam which flows out of the chimney of the PAR by natural convection. This reaction starts spontaneously at a hydrogen concentration of 1-2%, below the flammable hydrogen concentration of approximately 4%. The PARs are arranged throughout the containment structure. The rupture foils are placed in the ceiling structure above the SGs. They open passively when a pressure differential occurs and ensure global convection in the containment building. The hydrogen dampers are located in the bottom part of the containment, and they are stainless steel louvers. They reduce local hydrogen concentrations and prevent dangerously high concentrations associated with fast combustion by homogenizing the gas within the containment. They hydrogen dampers are fail safe due to the spring-loaded mechanism which opens automatically upon loss of power [3], [12], [13].

4.7. Core catcher

The core catcher catches the molten core material (corium) in case of meltdown, preventing the escape of corium to the environment [14]. The core catcher is made of thermally resistant concrete ceramic which does not melt when in contact with corium. In the EPR, the core catcher weighs 500t and had an area of 170 m² and is situated below the RPV. The core catcher is connected to the pressure vessel through a melt plug and a melt discharge channel. The melt plug is automatically destroyed when in contact with corium. The corium then flows into spreading compartment, where it is cooled by spreading in the available area. In order to cool down the corium more effectively, the spreading compartment can be flooded by water. The core catcher is made of cast iron elements with embedded cooling channels. A schematic of the core catcher is presented in Figure 13. [14]

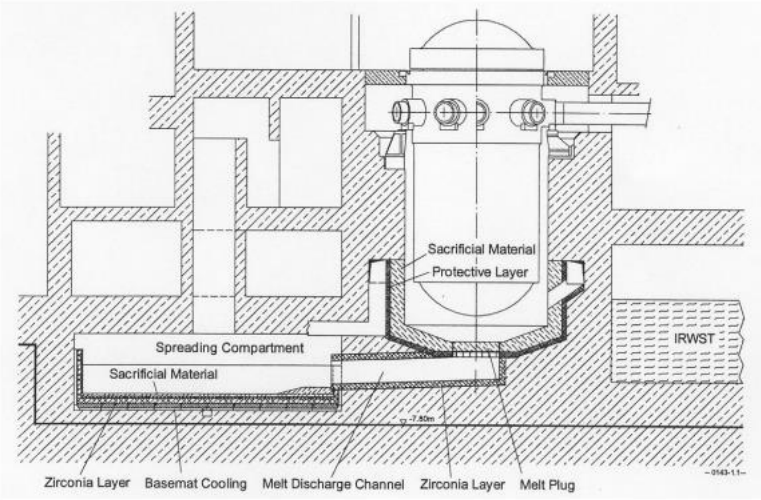

Figure 13 - Schematic of Core Catcher in EPR [15].

5. Calculation of Core Parameters

Key core parameters of the EPR are presented in Table 1. Note that a factor 1.05 is used for the total core heat output.

Table 1- Key Core Parameters of EPR

Parameter	**Value**	**Source**
Total core heat output	4725 MWth	[4]
Total core heat output in fuel	4465.125 MWth	[16]
Nominal system pressure	155 bar	[4]
Coolant inlet temperature	295.9°C	[4]
Coolant flow rate per fuel assembly	96.097 kg/s	[17]
Number of fuel assemblies	241	[4]
Number of fuel rods per assembly	265	[4]
Active fuel height	4.2 m	[4]
Lattice pitch	12.6 mm	[4]
Number of fuel rods per assembly	265	[4]
Outside fuel rod diameter	9.5 mm	[4]
Clad thickness	0.57 mm	[4]
Fuel pellet diameter	8.19 mm	[18]
Number of spacers, their locations and their local pressure loss coefficients	1 top spacer grid, 1 bottom spacer grid, and 10 mixing grids (uniformly distributed)	[4]
Clad wall roughness	0.001524 mm	[19]

5.1. Isolated Subchannel Model for PWR

The isolated subchannel model for a PWR was used to determine the mass flux, hydraulic diameter, and the heated perimeter, which were required for subsequent calculations. A schematic of the geometry of the subchannel for a square lattice is presented in Figure 14 [20].

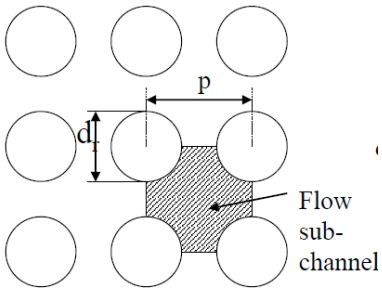

Figure 14 - Schematic of Square Lattice Subchannel Geometry

First, the subchannel area was determined from the subchannel geometry using Eq. 1 [20],

Eq. 1

$$A = p^2 - \frac{\pi {d_r}^2}{4},$$

where A is the subchannel area in m^2, d_r is the outer fuel rod diameter in m and p is the lattice pitch in m.

Since the coolant flow rate per fuel assembly is known, the ratio of the area of the subchannel to the entire area of the fuel assembly was used to determine the coolant flow rate per subchannel. Then, the mass flux was determined from Eq. 2 [20],

Eq. 2

$$G = \frac{W}{A},$$

where G is the mass flux in kg/m^2s and W is the coolant mass flow rate per subchannel in kg/s.

The heated perimeter was found from the channel geometry as presented in Eq. 3 [20],

Eq. 3

$$P_H = \pi d_r,$$

where P_H is the heated perimeter in m.

The hydraulic diameter was determined using the formula for the square lattice as presented in Eq. 4 [20],

Eq. 4

$$D_h = d_r \left[\frac{4}{\pi}\left(\frac{p}{d_r}\right)^2 - 1\right],$$

where D_h is the hydraulic diameter in m.

A summary of the results for these parameters in the EPR subchannel is presented in Table 2.

Table 2 - Subchannel Parameter Results for EPR

Subchannel Parameter	**Result**
Area, A	8.78778×10^{-5} m^2

Mass flux, G	3783.84 kg/m^{2}s
Heated perimeter, P_H	0.029845 m
Hydraulic diameter, D_h	0.011778 m

5.2. Core Power Distribution

The average linear power per fuel rod was determined from the total core power and the total number of fuel rods as presented in Eq. 5 [20],

Eq. 5

$$q'_{avg} = \frac{Q_{total\_core}}{N_{rod} \times L_{rod}},$$

where q'_{avg} is the average power per rod in W/cm, Q_{total_core} is the total core heat output in W, N_{rod} is the total number of fuel rods in the core, and L_{rod} is the active fuel rod length in cm.

The axial peaking factor of the core is determined using Eq. 6 [20],

Eq. 6

$$f_A = \frac{\pi H}{2\tilde{H} \sin\left(\frac{\pi}{2} \cdot \frac{H}{\tilde{H}}\right)},$$

where f_A is the axial peaking factor (unitless) and $H/\tilde{H}$ is the ratio of actual height to extrapolated height which is equal to 5/6 [16]. Only the axial peaking factor was used since radial power was assumed to be uniform in this calculation.

The maximum linear power per rod was then found using Eq. 7 [20],

Eq. 7

$$q'_0 = q'_{avg} \times f_A,$$

where q'_0 is the maximum power per rod in W/cm.

Finally, the linear power as a function of axial position was determined using Eq. 8 [20],

Eq. 8

$$q'(z) = q_0' \cos\left(\frac{\pi z}{\tilde{H}}\right),$$

where $q'(z)$ is the linear power of the fuel rod W/cm and z is the axial position (ranging from -H/2 to +H/2) in cm.

The core power distribution over the active fuel height for the EPR is presented in Figure 15. As expected, the power is highest in the centre of the core since that is where the neutron flux is at its maximum.

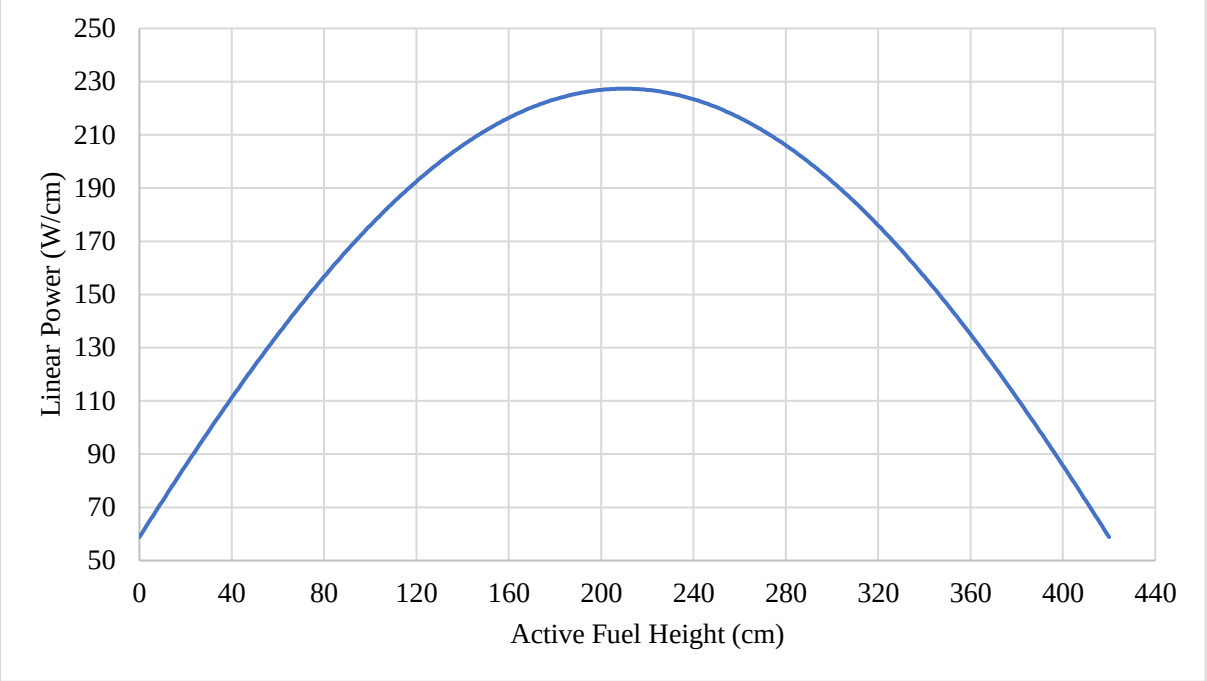

Figure 15- Core Power Distribution (Linear Power vs. Active Fuel Height) of the EPR

5.3. Axial Coolant Enthalpy Distribution

A nodalization approach was used to determine the coolant enthalpy distribution of the EPR. The fuel rod was divided into cells of 0.01 m in height. The inlet enthalpy was determined to be 1.315 x 10^6 J/kg·K from XSteam at the inlet conditions of 295.9°C and 155 bar. The enthalpy was then determined using Eq. 9 [20],

Eq. 9

$$i_j = i_{j-1} + \frac{q'_{j-1} \times z_{cell}}{W},$$

where i_j is the coolant enthalpy of cell j in J/kg, i_{j-1} is the coolant enthalpy of the previous cell in J/kg and z_{cell} is the cell height, 0.01 m.

The resulting coolant enthalpy distribution for the EPR is presented in Figure 16.

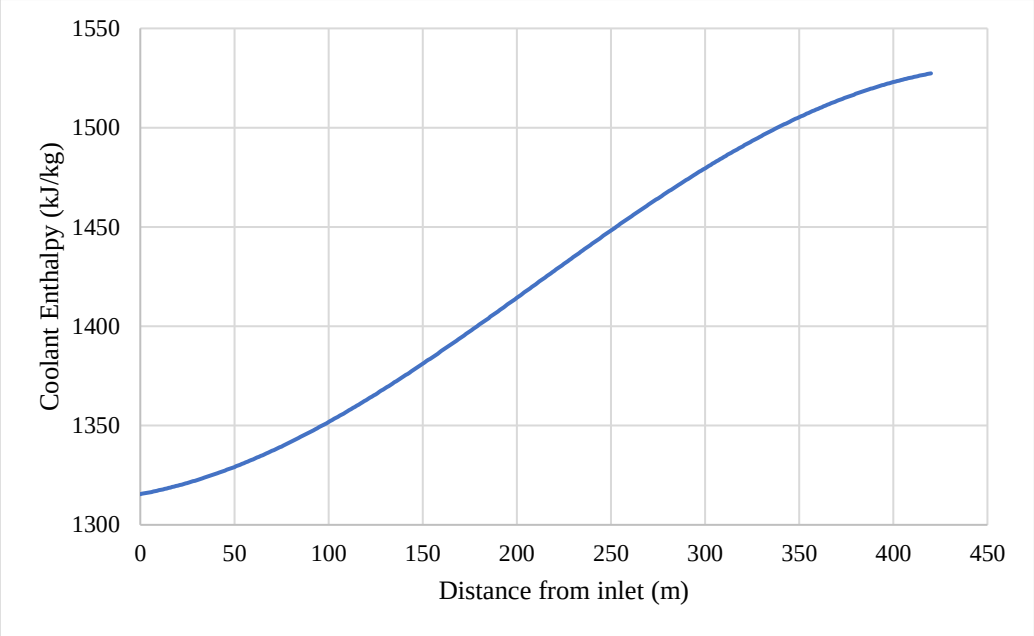

Figure 16 – Coolant Enthalpy Distribution of the EPR

The results in Figure 16 are as expected, given the cosine power distribution.

5.4. Axial Coolant Temperature Distribution

The same nodalization approach as described in Section 5.3 was used to determine the temperature distribution of the EPR. The temperature was determined using Eq. 10 [20].

Eq. 10

$$T_j = T_{j-1} + \frac{q'_{j-1} \times z_{cell}}{c_p W},$$

where T_j is the coolant temperature of cell j in °C, T_{j-1} is the coolant temperature of the previous cell in °C and c_p is the coolant heat capacity in J/kg°C.

The resulting coolant temperature distribution for the EPR is presented in Figure 16.

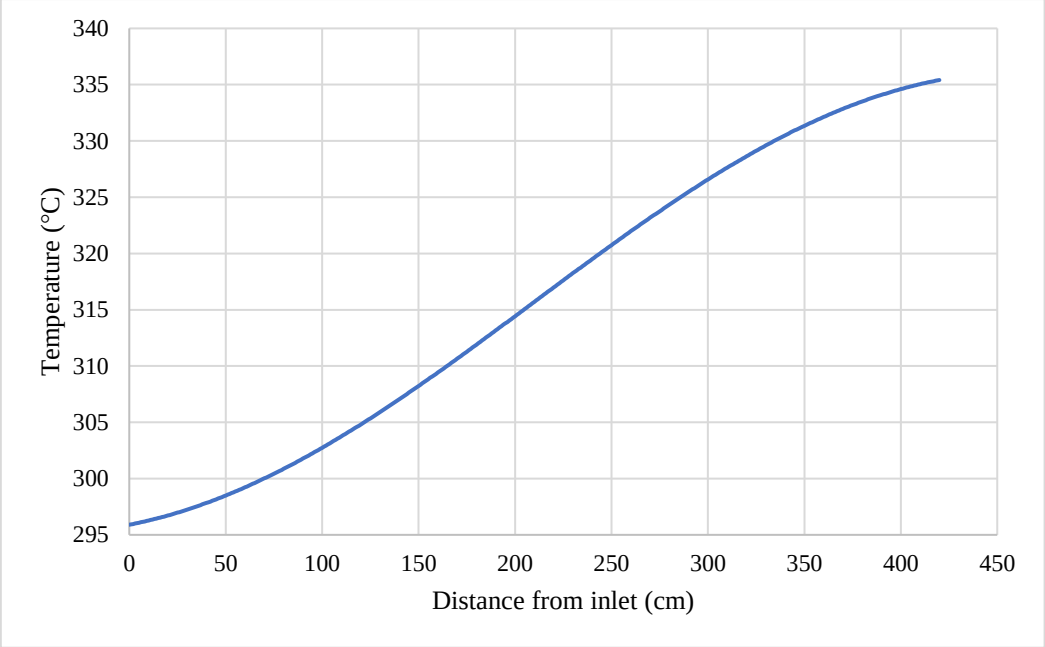

Figure 17 – Coolant Temperature Distribution of the EPR

The shape of the curve in Figure 17 is as expected, given the cosine power distribution. Table presents a comparison of the coolant outlet temperature from literature vs. the calculated values using 1.05 and 1.0 factors for power.

Table 3 – Comparison of coolant outlet temperature from literature and calculations.

Method	**Coolant Outlet Temperature (°C)**
From literature [4]	327.2
Calculated (1.05 power factor)	337.4
Calculated (1.0 power factor)	335.4

When the coolant outlet temperature was calculated using the linear power values determined from the 1.05 factor for power, there was a difference in coolant outlet temperature from literature of approximately 10°C. Initially, it was thought that this may be due to the power factor, so the coolant temperature was recalculated at nominal power (factor of 1.0) to see if this was the case. The coolant outlet temperature was still approximately 8°C higher than the literature value. Therefore, it was concluded that this is likely due to the equation used for power distribution. A generic equation was used as the specific power distribution equation for the EPR was not found. Further, the nodalization method was used which introduces inaccuracies when compared to the continuous temperature increase in the real reactor coolant.

5.5. Axial Pressure Drop Distribution

Since the EPR is a PWR, no boiling occurs so the coolant is always in the liquid phase at nominal flow rate and power. Therefore, the single-phase pressure drop equation was used as described by Eq. 11 [20]. Again, this was done using the nodalization method, so all equations described in this section were applied to individual cells.

Eq. 11

$$-\Delta p_{total} = -\Delta p_{friction} - \Delta p_{local} - \Delta p_{elev} = \left(\frac{4C_f H}{D_h} + \sum_i \xi_i\right)\frac{G|G|}{2\rho} + H\rho g,$$

where C_f is the friction coefficient (unitless), H is the distance from the inlet in m, ξ is the local loss coefficient (unitless), ρ is the coolant density (temperature dependent) in kg/m^3 and g is the gravitational constant of 9.81 m/s^2.

The Reynolds number was determined using Eq. 12 [20],

Eq. 12

$$Re = \frac{GD_h}{\mu},$$

where μ is the temperature-dependent dynamic viscosity in Pa.s.

The Haaland formula was used to determine the friction coefficient as presented in Eq. 13 [20],

Eq. 13

$$\frac{1}{\sqrt{C_f}} = -3.6\log_{10}\left[\left(\frac{k/D_h}{3.7}\right)^{1.11} + \frac{6.9}{Re}\right],$$

where k is the clad wall roughness in m.

The local loss coefficients used are presented in Table 4. It should be noted that the local loss coefficient for the inlet orifice was determined from 25% of the pressure drop as presented in Eq. 14 [16] [20],

Eq. 14

$$\xi_{orifice} = \frac{0.25 \times \Delta P \times 2\rho_f}{G^2}.$$

Table 4 - Values of local loss coefficient in EPR at various locations for calculation in average channel model.

Location	**Local loss coefficient**
Inlet orifice	3.84
Inlet	0.5
Outlet	1.0
Mixing spacer	$2 \cdot Re^{-0.08}$

The resulting axial pressure drop determined using Eq. 11 is presented in Figure 18.

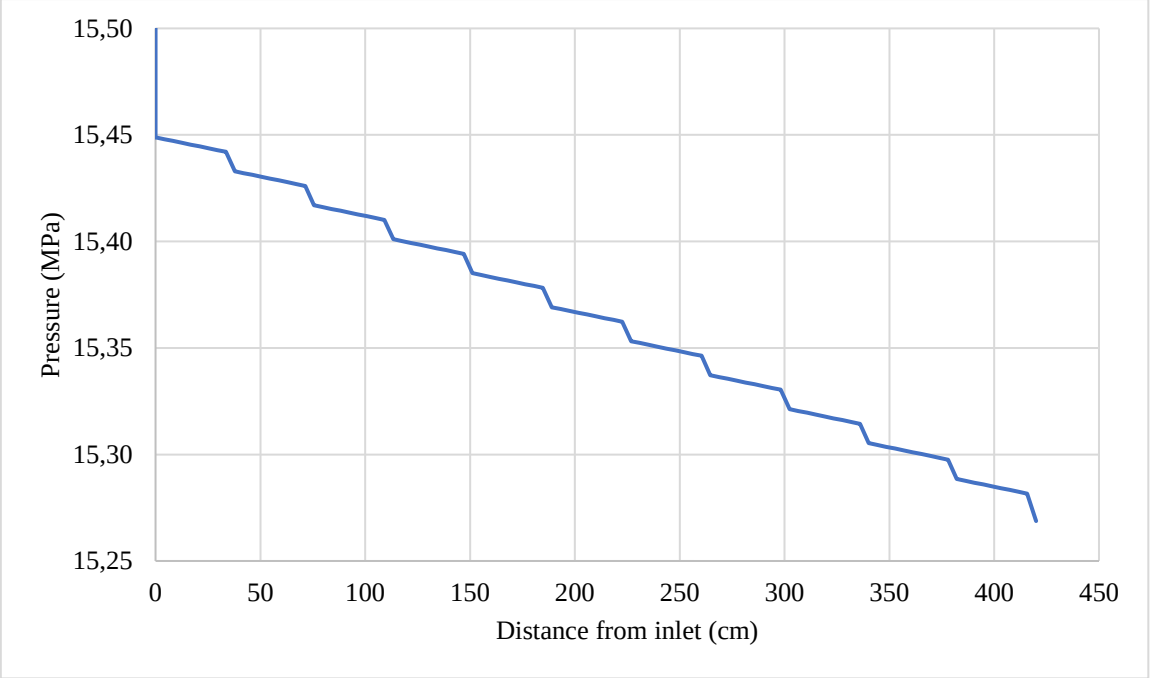

Figure 18 - Axial pressure distribution of the EPR

The total pressure drop was determined to be 0.231 MPa whereas in literature, the pressure drop was found to be 0.188 MPa. Since these values are reasonably close, it gives confidence in the calculation. Discrepancies likely arise due to the accuracies of correlations like the Haaland formula and the generic values/formulas for the local loss coefficients rather than using values specific to the EPR [17].

5.6. Flow Characteristics of the Core

The relationship between the axial pressure drop as a function of coolant mass flux was investigated at various power levels. Various combinations of mass flux and power (i.e. low mass flux and high power) resulted in the introduction of two-phase flow. The quality in these regions was calculated according to Eq. 15 [21],

Eq. 15

$$x(z) = \frac{i(z) - i_f}{i_{fg}},$$

where $x(z)$ is the quality according to axial position (unitless), i_f is the enthalpy of the liquid at saturation in J/kg and i_{fg} is the enthalpy of evaporation in J/kg.

With the introduction of boiling, the pressure drop calculations were performed differently. Namely, the Homogeneous Equilibrium Model (HEM) was used to calculate the density and dynamic viscosity of the liquid-vapour mixture, as presented in Eqs. 16 and 17, respectively [22].

Eq. 16

$$\rho_m = \frac{\rho_f}{x\left(\frac{\rho_f}{\rho_g} - 1\right) + 1},$$

Eq. 17

$$\frac{1}{\mu_m} = \frac{x}{\mu_g} + \frac{1-x}{\mu_f},$$

where the subscript *m* represents the mixture properties, *g* represents the properties of the vapor at saturation, and *f* represents the properties of the liquid at saturation.

The same approach to calculate pressure drop was used as presented in Section 5.5, however μ_m was used in the Reynolds number calculation and ρ_m was used in the pressure drop equation in the regions of two-phase flow (i.e. where x > 0). Additionally, the acceleration pressure drop had to be accounted for in the two-phase flow regions. The acceleration pressure drop is a result of the density change of the fluid during the evaporation process and is represented by Eq. 18 [22].

Eq. 18

$$-\Delta p_{acc} = \frac{G^2}{2\rho_m},$$

The pressure drop from 1% to 150% mass flux at 0%, 50%, 100% and 150% nominal power are presented in Figure 19.

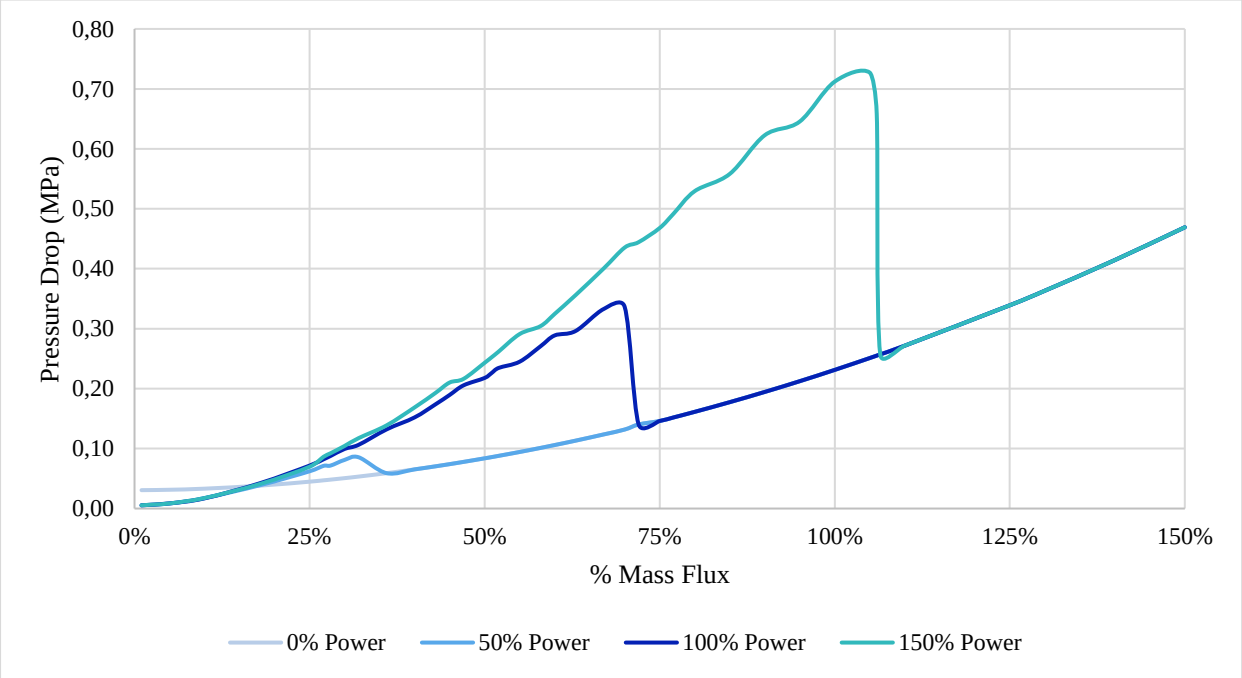

Figure 19 - Pressure drop as a function from 1% to 150% mass flux at 0%, 50%, 100% and 150% nominal power

In the low mass flux region (~1 – 10%), the coolant is in the gas phase at every power except 0%, therefore the pressure drop at 50, 100 and 150% is higher than 0%, which is fully in liquid form. As the mass flux continues to increase, the pressure drop at 50, 100 and 150% power increases in comparison to 0% power, since two-phase flow is introduced. When the mass flux is reached where boiling no longer occurs (i.e. the coolant is fully liquid) for each respective power, there is a drastic decrease in the pressure drop and it converges with the 0% power pressure drop. At a mass flux of 107% and higher, the pressure drop for all power levels is approximately the same since the coolant in fully in the liquid phase in this region.

We can see fluctuations in pressure drop in the two-phase flow regions due to the Ledinegg instability. The Ledinegg instability says that the pressure drop in a boiling channel is lower when the flow is fully liquid when compared to fully steam. As the flow rate increases and the flow transitions from gas to the liquid state, instabilities are introduced as shown in the curve from the "all vapor" to "all liquid" curves in Figure 20 [23].

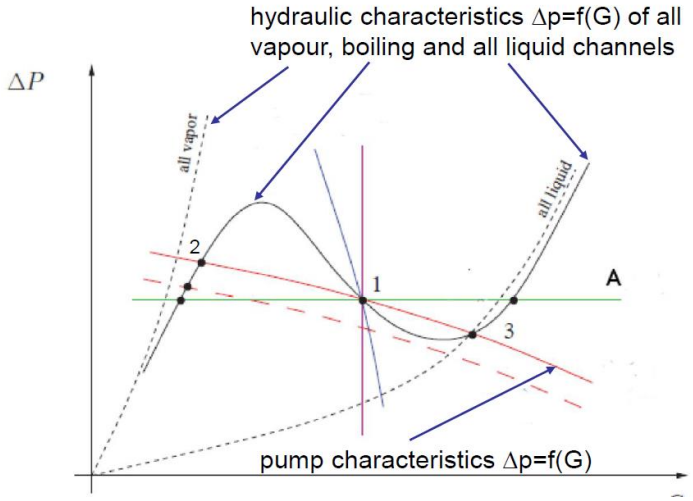

Figure 20 - Illustration of Ledinegg Instability Concept

6. Calculation of CHF Margins in a Hot Channel

The calculations in this section follow a similar approach to those discussed in Section 5, however, core power distribution in the hot channel was used instead of the average channel. Parameters used for all the calculations are the same as presented in Table 1 and the ones calculated with Isolated Subchannel Model in Section 5.1.

6.1. Hot Channel Configuration

In contrast with the power distribution in average channel configuration, the peaking factor used to determine the maximum power considered both radial and axial peaking factor. This is because in the hot channel, it is not assumed that the radial power density is uniform. In hot channel conditions, we can study the situation when the flux is the higher in the channel and we can identify some important safety points that should be monitored.

To determine the power density distribution, we used the average linear power per fuel rods, q'_{avg} that was determined from the total core power and the total number of fuel rods previously with Eq 5 [20]. In the hot channel, the maximum linear power per rod was found using Eq. 19,

Eq. 19

$$q'_{0,hot} = q'_{avg} \times f_A \times f_R,$$

where $q'_{0,hot}$ is the maximum power per rod in the hot channel in W/cm, and f_R is the radial peaking factor determined by Eq. 20,

Eq. 20

$$f_R = \frac{2.405R}{2\tilde{R}J_1\left(\frac{2.405R}{\tilde{R}}\right)},$$

where $R/\tilde{R}$ is the ratio of actual radius to extrapolated radius which is equal to 5/6 [16].

The global peaking factor is the product of the radial and the axial peaking factors. The peaking factor values used in this study are presented in Table 5.

Table 5 – Summary of peaking factor values

Axial peaking factor/ Average channel peaking factor (-)	1.35
Radial peaking factor (-)	1.74
Hot channel peaking factor (-)	2.35

Finally, the linear power as a function of axial position was determined as before, using Eq. 8 [20]. The core power distribution obtained with hot channel configuration and with average channel configuration over the active fuel height for the EPR are presented in Figure 21.

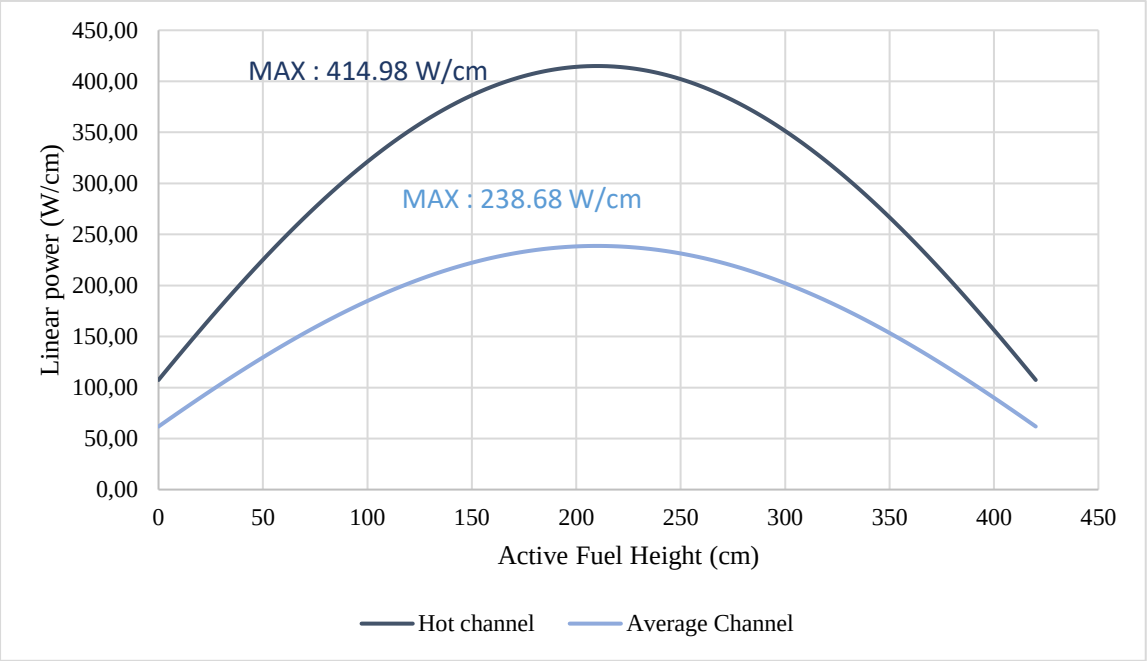

Figure 21 – Power density axial distribution in hot channel configuration

As expected, the hot channel power density distribution follows the same shape as the average configuration and the position of maximum power corresponds to the centre of the rod. The ratio between the two maximum linear power obtain for each configuration is equal to the ratio between the peaking factor that are applied in each case, 1.76.

6.2. Coolant Enthalpy Axial Distribution

As in Section 5.3, the coolant enthalpy evolution has been calculated through a nodalization approach. The number of cells used to divide the rods into small parts was kept the same. Inlet enthalpy did not depend on the power distribution and was kept the same as for average channel, 1.315 x 10^6 J/kg·K (XSteam at 295.9°C and 155 bar). The enthalpy was then determined using Eq. 9 and its distribution is plotted in Figure 22.

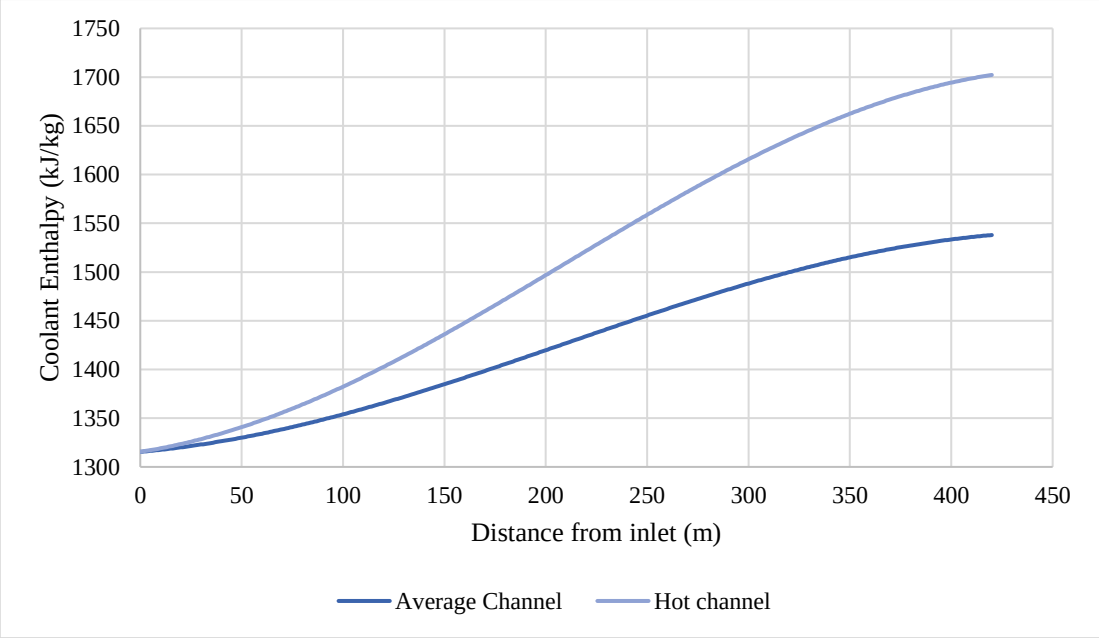

Figure 22 – Axial Coolant Enthalpy Distribution in Average and Hot Channel

We could observe in Figure 22 that the coolant enthalpy axial distribution has the same shape in both the average and hot channel configurations. The maximum coolant enthalpy value has increased in the hot channel configuration to 1702.2 kJ/kg.

6.3. Coolant temperature axial distribution

The nodalization approach continued to be used to determine the temperature distribution of the hot channel. To determine the evolution of temperature we had simply used the XSteam function that gives temperature as a function of enthalpy and pressure. To use this function, pressure was fixed at 155 bar and enthalpy is taken according to the distribution presented in Figure 22. The resulting coolant temperature distribution for the EPR in hot channel configuration is presented in Figure 23.

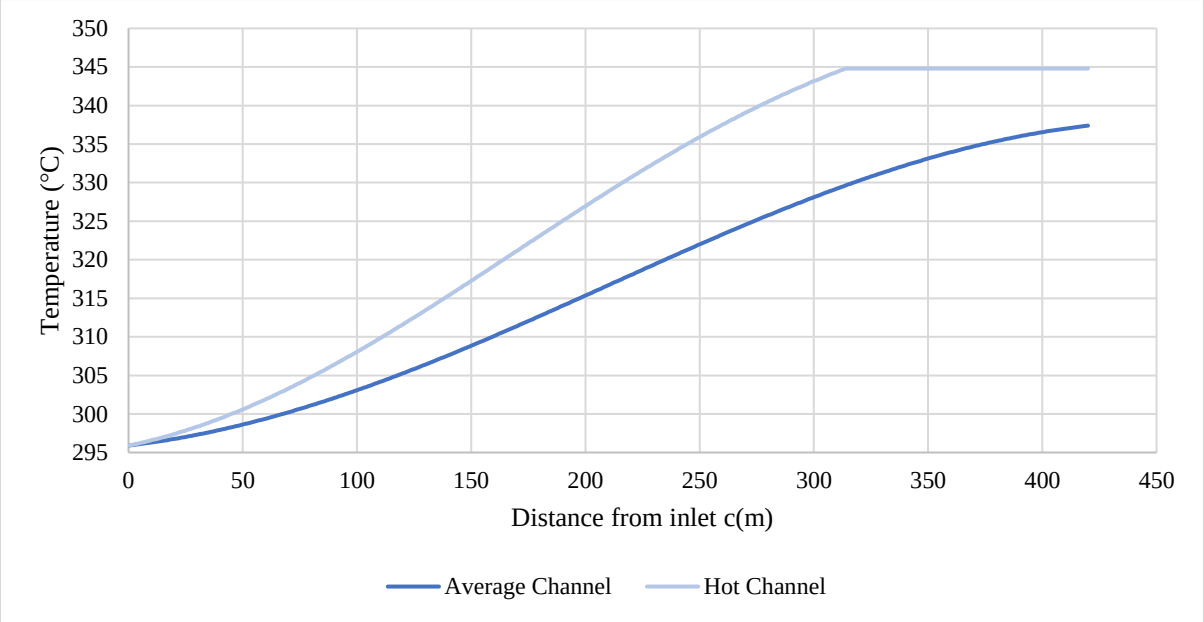

Figure 23 - Axial Coolant Enthalpy Distribution in Average and Hot Channel

In Figure 23, we could observe that the temperature distribution plotted by using hot channel follow the same shape as the temperature distribution from Figure 17 with higher temperature values until z = 314 cm. At this point, the coolant reached its saturation temperature of 344.79 °C. This effect is because the saturation liquid enthalpy from EPR has been exceeded and steam begins to form in the reactor. Nevertheless, the temperature did not continue to grow because the enthalpy is transformed to latent heat rather than sensible heat.

6.4. Pressure Drop

The EPR pressure drop in the hot channel configuration was calculated using same methods as in Sections 5.5 and Sections 5.6 since there are regions of both single and two-phase flow. The resulting axial pressure drop distribution is plotted Figure 24.

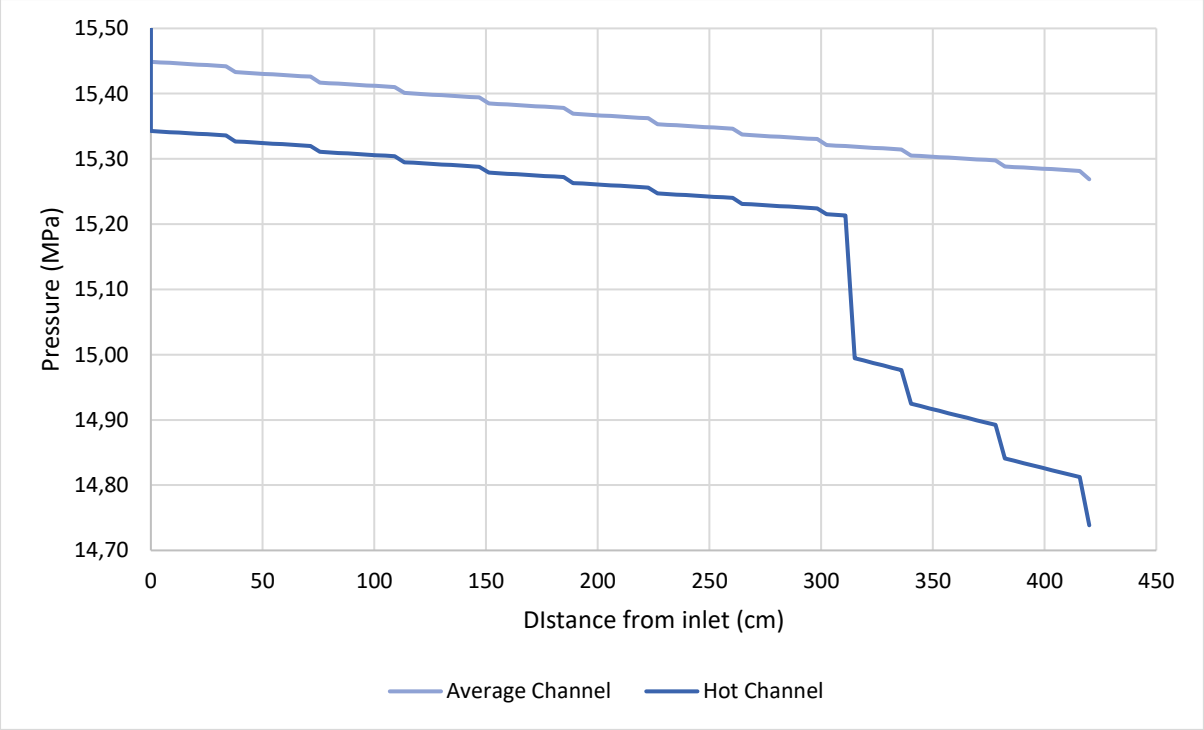

Figure 24- Axial pressure distribution of the EPR in hot channel and average configurations

When the coolant is fully in the liquid state (z < 314 cm), the pressure drop follows the same evolution in the hot channel configuration than in the average channel configuration. This observation aligns with the results in Figure 19, as we have observed that in the single-phase flow region, the pressure drop is not significantly influenced by the reactor power. Nevertheless, when two phase flow begins, the pressure drop increases. The important decrease that can be observe at z = 314 cm could be due to a hot spot as it correspond to the position where the coolant temperature is at its maximal value. After that as we were over the saturation temperature more and more steam will be created and so pressure drop will continue to decrease but with smaller steps.

In Figure 24, the inlet pressure drop is larger in the hot channel configuration because it is calculated via the orifice local loss coefficient that dependent on the total pressure drop. This coefficient value in the hot channel configuration is around 12.6 when in average channel configuration it is about 3.8.

Finally, the total pressure drop in hot channel configuration is about 0.76 MPa which is almost 4 times the pressure drop in the average channel. This difference seems logical as in the hot channel configuration, there is the presence of two-phase flow which has a significant influence on the pressure drop.

6.5. DNBR and MDNBR calculations

The departure from nucleate boiling (DNB) in PWRs is an important safety parameter that must be considered. The DNR ratio (DNBR) is defined by the Eq. 21,

Eq. 21

$$\mathrm{DNBR} = \frac{q_{CR}''(z)}{q''(z)},$$

where $q_{cr}''(z)$ is the local critical power in hot channel and $q''(z)$ is the local actual heat flux in hot channel, both in W/m^2.

The critical power in hot channel was calculated using the Subchannel CHF Correlation presented in Eq. 22,

Eq. 22

$$q_{CR}''(z) = B\,\frac{A - x_{in}}{C + \frac{x(z) - x_{in}}{q_R''(z)}},$$

where B = 3.1544 x 10^6, A and C are constants that are respectively defined by Eq. 23 and Eq. 24, x_{in} is the inlet quality, $x(z)$ is the quality at location z and $q''_R(z)$ is a power parameter in W/m^2 defined by Eq. 25.

Eq. 23

$$A = a_1 \times \left(\frac{p}{p_{cr}}\right)^{a_2} \times \left(\frac{G}{1356.23}\right)^{\left(a_3 + a_4 \times \frac{p}{p_{cr}}\right)},$$

where p is the pressure in the system in Pa, p_{cr} is the critcial pressure for an EPR (22.1 x 10^6 Pa), a_1 = 0.5328, a_2 = 0.1212, a_3 = -0.3040 and a_4 = 0.3285.

Eq. 24

$$C = c_1 \times \left(\frac{p}{p_{cr}}\right)^{c_2} \times \left(\frac{G}{1356.23}\right)^{\left(c_3 + c_4 \times \frac{p}{p_{cr}}\right)},$$

where c_1 = 1.6151, c_2 = 1.4066, c_3 = 0.4843 and c_4 = -2.0749.

Eq. 25

$$q_R''(z) = \frac{q''(z)}{3.1544e6},$$

Conditions to apply this correlation are presented in Table 6. While this correlation did not fulfil the requirements for the mass flux, there were no correlations provided that met all of the criteria for the EPR so this model was selected as a best estimate.

Table 6 – Validity criteria for CHF correlation

Criteria	EPR parameter	Parameter check
147 < G < 3023 kg/m²s	G = 3783 kg/m²s	
13.8 < p < 169.9 bar	p = 155 bar	Valid
8.9 < D_h < 13.9 mm	D_h= 11,8 mm	Valid
-0.25 < x < 0.75	-0.32 < x < 0.07	Valid after z = 1.05 m
-1.10 < x_{in} ≤ 0.0	x_{in} = -0.32	Valid
0.762<L<4.267 m	L = 4.2 m	Valid

The resulting DNBR axial distribution is presented in Figure 25.

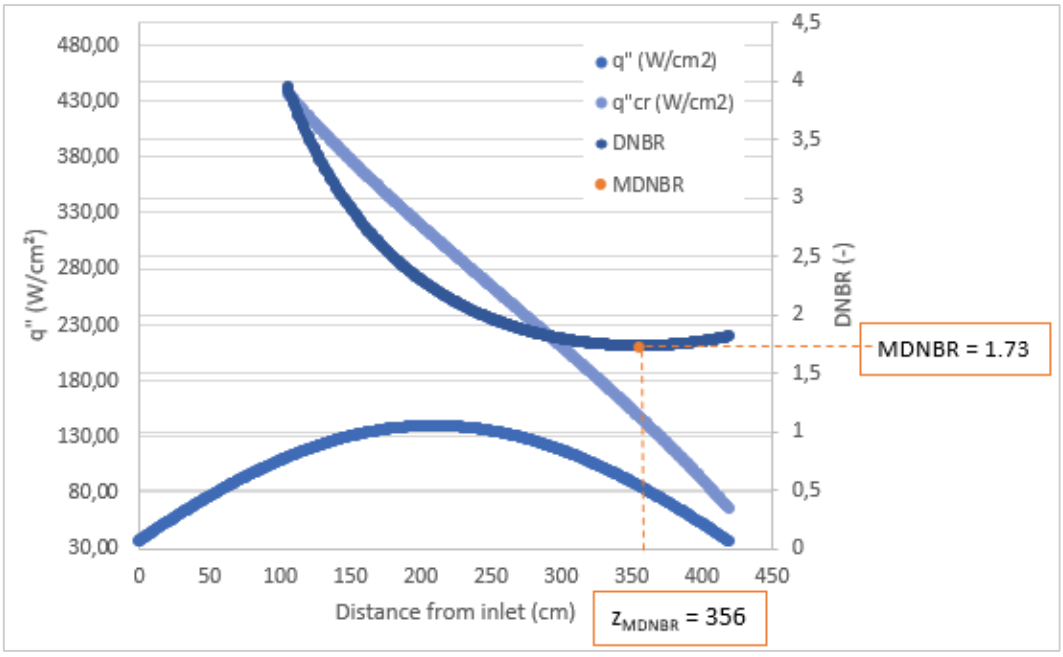

Figure 25- Axial distribution of DNBR for an EPR

From Figure 25, we can extract the minimum DNBR (MDNBR) value which is 1.73 and corresponds to the position z = 3.56 m. This MDNBR provides a high safety margin because even in the hot channel configuration, the minimum critical heat flux causing DNB occurs at a point where it is 173% higher than the local heat flux which is unlikely.

6.6. Avoiding Boiling

The previous calculation presents problems as in a hot channel configuration, it seems that coolant will exceed its saturation temperature, so steam will be generated. Nevertheless, steam should not be present in a PWR otherwise fuel damage will occur. Table 7 presents search for a power configuration at which the EPR will never reach its saturation temperature.

Table 7 – Power study for avoiding boiling.

Power [MWth]	Final temperature (°C)	Location where T_{sat} is reached (m)
4725	344.7915	3.14
4500	344.7915	3.31
4050	344.7915	3.78
3825	344.6328	X
3600	342.4959	X

From the results in Table 7 it has been determined that to prevent boiling in the hot channel configuration, the power should be decreased 900 MWth to a total power of 3825 MWth.

7. Calculation of the Maximum Cladding and Fuel Pellet Temperature

To maintain reactor safety, it is critical for the fuel and cladding temperatures to remain below the melting point of the material. In this task, the "hot spot" temperatures and locations of the fuel and cladding are determined to ensure design limitations are not exceeded.

In the single-phase regions, the Nusselt number, *Nu*, of the coolant was determined using the Dittus-Boelter equation for heating shown in Eq. 26 [24],

Eq. 26

$$Nu = 0.023Re^{0.8}Pr^{0.4},$$

where *Pr* is the Prandtl number which is defined by Eq. 27 [24],

Eq. 27

$$\Pr = \frac{c_p \mu}{\lambda},$$

where λ is the thermal conductivity of the coolant in W/mK. It should be noted that all properties of the coolant are temperature dependent.

The Nusselt number of the whole fuel bundle in the single-phase regions, Nu_{bundle}, was then found using Eq. 28 [24],

Eq. 28

$$Nu_{bundle} = Nu_{DB}\left(1 + 0.91Re^{-0.1}Pr^{0.4}(1 - 2e^{-B})\right),$$

where *B* for a square lattice is defined by Eq. 29 [24],

Eq. 29

$$B = \frac{4}{\pi}\left(\frac{p}{d_r}\right)^2 - 1.$$

The single-phase heat transfer coefficient of the coolant, h_{lo} (W/m^{2}K), was then found using Eq. 30 [24],

Eq. 30

$$h_{lo} = \frac{Nu_{bundle} \times \lambda}{D_h}.$$

For regions where boiling occurs, the two-phase heat transfer coefficient, $h_{2\phi}$, was determined using the Collier and Pulling correlation presented in Eq. 31 [25],

Eq. 31

$$h_{2\phi} = h_{lo}\left(6700\frac{q''}{Gi_{fg}} + 2.34X_{tt}^{-b}\right),$$

where X_{tt} is the Martinelli parameter presented in Eq. 32 [25],

Eq. 32

$$X_{tt} = \left(\frac{1-x}{x}\right)^{0.9}\left(\frac{\rho_g}{\rho_f}\right)^{0.5}\left(\frac{\mu_f}{\mu_g}\right)^{0.1}.$$

The thermal conductivity of the fuel, λ_F (W/mK), was determined using Eq. 33 [24],

Eq. 33

$$\lambda_F = \frac{100}{7.5408 + 17.692t + 3.6142t^2} + \frac{6400}{t^{5/2}}exp\left(-\frac{16.35}{t}\right),$$

where $t = T/1000$ and T is temperature in K and a fuel porosity of 5% is assumed.

The thermal conductivity of the M5 cladding, λ_C (W/mK), was determined from Eq. 34 [26],

Eq. 34

$$\lambda_C = 15.0636 \times e^{0.000461843T}.$$

The thermal conductivity of the helium gas gap was determined using Eq. 35 [27],

Eq. 35

$$\lambda_G = 0.0476 + 0.362 \cdot 10^{-3}T - 0.618 \cdot 10^{-7}T^2 + 0.718 \cdot 10^{-11}T^3$$

Heat convection from the coolant to the cladding and heat conduction through the cladding, gas gap and fuel was used to determine the temperature at different surfaces throughout the fuel rod. Figure 26 shows the geometry used in the conduction equations where r_{Fo} is the outer radius of the fuel pellet, r_{Go} is the outer radius of the gas gap, and r_{Co} is the outer radius of the cladding.

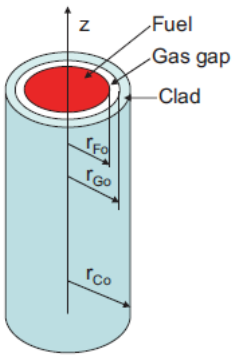

Figure 26 - Geometry of Fuel Rod

The values of the outer radii used are presented in Table 8.

Table 8 - Fuel, gas gap, and cladding outer radius values

r_{Fo}	4.095 mm
r_{Go}	4.18 mm
r_{Co}	4.75 mm

The fuel centreline temperature, T_{Fc}, is determined from the sum of the coolant temperature, T_{lb} and the whole fuel rod temperature change as shown in Eq. 36 [24],

Eq. 36

$$T_{Fc} = T_{lb} + \frac{q'}{4\pi}\left[\frac{1}{\lambda_F} + \frac{2}{\lambda_G}\ln\left(\frac{r_{Go}}{r_{Fo}}\right) + \frac{2}{\lambda_C}\ln\left(\frac{r_{Co}}{r_{Go}}\right) + \frac{2}{r_{Co}h}\right].$$

The outer fuel pellet temperature, T_{Fo}, is determined from the difference of the fuel centreline temperature and the temperature change in the fuel pellet as shown in Eq. 37 [24].

Eq. 37

$$T_{Fo} = T_{Fc} - \frac{q''' r_{Fo}^2}{4\lambda_F}.$$

The inner cladding temperature, $T_{Ci,}$ is determined from the difference of the outer fuel pellet temperature and the temperature change in the gas gap as shown in Eq. 38 [24],

Eq. 38

$$T_{Ci} = T_{Fo} - \frac{q''' r_{Fo}^2}{2\lambda_G} \ln\left(\frac{r_{Go}}{r_{Fo}}\right).$$

The maximum cladding temperature will be located at the cladding inner surface since it is closest to the fuel. Figure 27 presents the axial distribution of fuel centreline and cladding inner temperature.

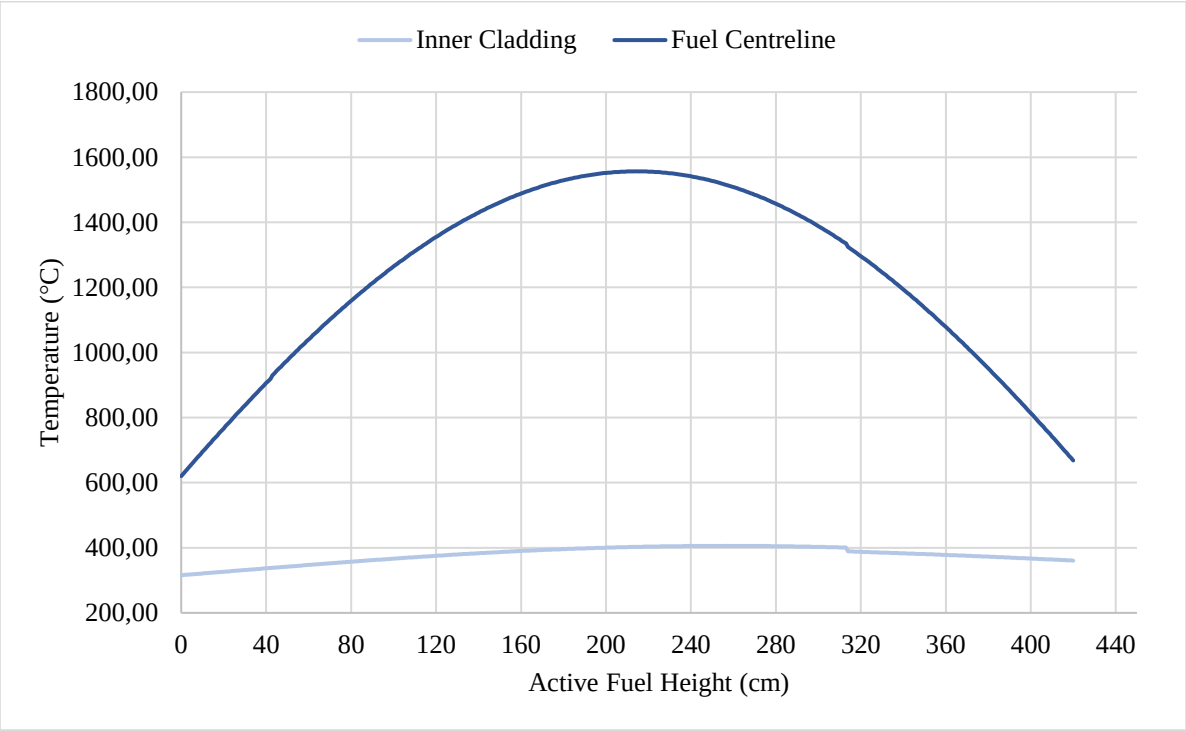

Figure 27 - Axial Distribution of Inner Cladding and Fuel Centreline Temperature

As shown in Figure 27, there is a small jump in temperature at 314 cm. This is because this is the point where two-phase flow is introduced so the heat transfer coefficient changes rather significantly at this point, influencing the shape of the temperature curves.

Figure 28 presents the radial distribution of the temperature at the point of the maximum fuel centreline temperature determined from the axial distribution (active fuel height of 214 cm).

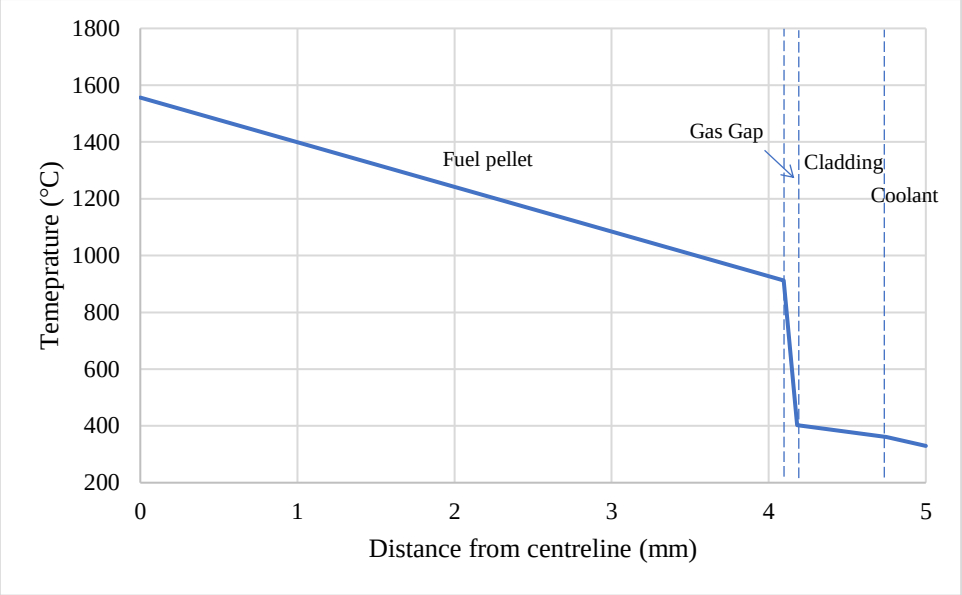

Figure 28 - Radial Temeprature Distribution at Height of 214 cm

The results of the maximum fuel centreline and cladding temperatures and their respective positions ("hot spot" temperatures and positions) are compared to the melting point of the fuel and cladding materials in Table 9.

Table 9 - Hot spots temperatures and location and melting points of cladding and fuel.

	Inner Cladding	**Fuel centreline**
Hot spot temperature (°C)	405.8	1556.5
Melting point of material (°C)	1855	2878
Hot spot location (cm)	257	214

The results in Table 9 show that the maximum cladding and fuel temperatures are far from the melting points of the material, therefore there is a large margin for core meltdown.

8. References

[1] Wikipedia, ”EPR (nuclear reactor),” 2023. [Online]. Available: https://en.wikipedia.org/wiki/EPR_(nuclear_reactor). [Använd 31 January 2023].

[2] R. Leverenz, L. Gerhard och A. Göbel, ”The EUropean Pressurized Reactor: A Safe and Competitive Solution for Future Energy Needs,” Nuclear Energy for New Europe 2004, Ljubljana, 2004.

[3] UK-EPR, ”Fundamental Safety Overview,” AREVA NP & EDF, 2007.

[4] AREVA, ”EPR,” 20 May 2005. [Online]. Available: https://web.archive.org/web/20071129121411/http://www.areva-np.com/common/liblocal/docs/Brochure/EPR_US_%20May%202005.pdf.

[5] USNRC, ”Backgrounder on High Burnup Spent Nuclear Fuel,” September 2018. [Online]. Available: https://www.nrc.gov/reading-rm/doc-collections/fact-sheets/bg-high-burnup-spent-fuel.html. [Använd 1 February 2023].

[6] C. Zeng, M. Wang, G. Wu och S. Yin, ”Numerical study on the enhanced heat transfer characteristics of steam generator with axial economizer,” *International Journal of Thermal Sciences,* 2022.

[7] UK-EPR, ”PCSR – Sub-chapter 18.2 – Normal Operation,” 2012.

[8] F. PAIROT, ”EPR : HIGH LOAD VARIATION PERFORMANCES WITH THE "TMODE” CORE CONTROL,” AREVA, 2008.

[9] IRSN, ”Design and Operation of a Pressurised Water Reactor”.

[10] NRC, ”Westinghouse Technology Systems Manual : Chemical and Volume Control System”.

[11] AREVA, ”EPR™ Safety Systems,” 2010.

[12] ”Passive Autocatalytic Recombiners,” Wikipedia, 2022. [Online]. Available: https://en.wikipedia.org/wiki/Passive_autocatalytic_recombiner. [Använd 7 February 2023].

[13] Framatome, ”Hydrogen Mixing Dampers,” [Online]. Available: https://www.framatome.com/solutions-portfolio/docs/default-source/default-document-library/product-sheets/a1711-p-ge-g-en-1711-201901-hydrogen-mixing-dampers.pdf?sfvrsn=1e8754f4_2. [Använd 7 February 2023].

[14] M. Pikkarainen, ”Heat Transfer Analysis of the European Pressurized Water Reactor (EPR) Core Catcher Test Facility Volley,” 2008.

[15] AREVA, ”Technical Evolution of the EVR Melt Stabilization Concept for the EPR,” 2016.

[16] P. Kudinov, *SH2702 Project work description,* Stockholm: KTH Royal Institute of Technology, 2023.

[17] M. Skrzypek och R. Laskowski, ”Thermal-hydraulic calculations for a fuel assembly in a European Pressurized Reactor using the RELAP5 code,” Warsaw University of Technology, Warsaw, 2015.

[18] UK EPR, ”FUNDAMENTAL SAFETY OVERVIEW”.

[19] Framatome ANP, Inc., ”Incorporation of M5 TM Properties in Framatome ANP Approved Methods,” United States Nuclear Regulatory Commission, 2002.

[20] H. Li, *SH2702 Nuclear Reactor Technology Project Work Task 4,* Stockholm: KTH Royal Institute of Technology, 2023.

[21] H. Anglart, ”TH Design of Fuel Assemblies with Single-Phase Coolant Pressure Drop and DNB,” KTH Royal Institute of Technology, Stockholm, 2022.

[22] H. Anglart, ”Void Fraction and Pressure Drop,” KTH Royal Institute of Technology, Stockholm, 2022.

[23] H. Anglart, *Stability of Boiling Channels,* Stockholm: KTH Royal Institute of Technology, 2022.

[24] H. Li, *SH2702 Porject Work Task 6,* Stockholm: KTH Royal Institute of Technology, 2023.

[25] H. Anglart, *Saturated Boiling, Dryout and Post-dryout Heat Transfer,* Stockholm: KTH Royal Institute of Technology, 2022.

[26] A. Kecek, ”Development of M5 Cladding Material Correlations in the TRANSURANUS Code,” JRC Publications, Luxembourg, 2016.

[27] N. Vargaftik, ”Temperature Dependence of Thermal Conductivity of Helium,” Plenum Publishing Corp., New York, 1976.